

# Investigating the impact of sub-ice shelf melt on ~~Antarctica Ice Sheet~~ the Antarctic ice sheet spin-up and projections

Fan Gao<sup>1,2</sup>, Qiang Shen<sup>1,2</sup>, Hansheng Wang<sup>1,2</sup>, Tong Zhang<sup>3</sup>, Liming Jiang<sup>1,2</sup>, Yan Liu<sup>4</sup>, C.-K. Shum<sup>5</sup>, Yan An<sup>1,2</sup>, and Xu Zhang<sup>1,2</sup>

5 <sup>1</sup>State Key Laboratory of Precision Geodesy, Innovation Academy for Precision Measurement Science and Technology, Chinese Academy of Sciences, Wuhan 430077, China

<sup>2</sup>College of Earth and Planetary Sciences, University of Chinese Academy of Sciences, Beijing 100049, China

<sup>3</sup>State Key Laboratory of Earth Surface Processes and Disaster Risk Reduction, Faculty of Geographical Science, Beijing Normal University, Beijing 100875, China

10 <sup>4</sup>State Key Laboratory of Remote Sensing Science, College of Global Change and Earth System Science, Beijing Normal University, Beijing 100875, China

<sup>5</sup>Division of Geodetic Science, School of Earth Sciences, The Ohio State University, Columbus, Ohio, 43210, USA

*Correspondence to:* Qiang Shen (cl980606@whigg.ac.cn) and Tong Zhang (tongzhangice@gmail.com)

**Abstract.** Sub-ice shelf melting is critical for the stability of the Antarctic Ice Sheet, as it influences ice-shelf buttressing that ~~impedes~~reduces grounded ice flow. Previous studies have emphasized that uncertainties in the state of sub-ice shelf melting contribute to ~~inaccuracies~~uncertainties in future sea-level projections. To better understand how sub-ice shelf melt rates affect model initialization and predictions, we adopt a single ice-sheet model (PISM) and investigate two different sub-ice shelf melt rate schemes during model spin-ups. We then drive the Antarctic Ice Sheet into the future using identical environmental forcings. We find that, despite closely matched steady-state geometries achieved through the spin-up process with different sub-ice shelf melt rates, the prognostic simulations reveal significantly divergent ice mass changes, particularly in marine ice sheet regions. By 2100, the difference in global sea-level contributions from the Antarctic Ice Sheet can be as large as ~57%, primarily from West Antarctica. This discrepancy arises because the spin-up initialization method alters the ice sheet's dynamic state, such as basal friction and thermal regimes, leading to varied ice-sheet mass changes. Therefore, this study underscores the importance of sub-ice shelf melting and ice-sheet model initialization methods in reducing uncertainties in predicting the Antarctic Ice Sheet's future.

## 1 Introduction

A substantial majority of Antarctica's grounded ice ~~discharges~~discharges through its fringing ice shelves, which provide critical buttressing to upstream ice mainly through two primary mechanisms: lateral shear stresses along sidewalls and basal resistance forces at pinning points on topographic highs (Schoof, 2007; Goldberg et al., 2009; Feldmann & Levermann, 2023; Feldmann et al., 2024; Miles & Bingham, 2024). ~~The exposure of ice~~Ice shelves ~~to~~are

~~highly vulnerable to oceanic forcing due to warm seawater causes basal melting, combined with their~~ near-flotation elevation ~~exposes them to warm seawater, which causes enhanced basal melting, resulting in high susceptibility to oceanic forcing~~ (Bindschadler et al., 2013; Depoorter et al., 2013; Li et al., 2023). Observations reveal accelerating ocean-driven thinning of Antarctic ice shelves over recent decades (Paolo et al., 2015; Rignot et al., 2019), where enhanced basal melting reduces buttressing effects and promotes grounding-line retreat, which collectively ~~represents~~ represent the primary driver of increased ice discharge (Jacobs et al., 2011; Pritchard et al., 2012; Seroussi et al., 2014; Jourdain et al., 2020; Reese et al., 2020). Particularly on retrograde bed slopes, such retreat may trigger Marine Ice Sheet Instability (MISI), ~~which has been observed to increase grounded ice velocities by 34% (Rignot a~~ critical feedback mechanism that is often identified as a decisive factor in the collapse of the West Antarctica (Schoof, 2007; Hill et al., 2008) and 2024). This process may ~~amplify~~ amplify ice loss by up to Antarctic contribution to global sea-level rise by 0.65 to 0.8 meters of sea level equivalent (m SLE) this century (DeConto & Pollard, 2016; ~~Schlemm~~ Ritz et al., 20222015).

Methods for ice-sheet models to represent sub-ice shelf melting include linear non-linear and local/non-local dependency thermal forcing (~~TF linear~~ parameterization parameterizations) (Martin et al., 2011; Favier et al., 2019; Lowry et al., 2021), ice-shelf cavity models developed from box or plume models (Lazeroms et al., 2018; PICO, Reese et al., 2018; Favier et al., 2019; PICOP, Pelle et al., 2019), empirical approximations (Cornford et al., 2015; Cornford et al., 2020), basin-averaged melt estimates (Seroussi et al., 2019), and spatially partitioned quadratic parameterization parameterizations (ISMIP6 protocol, Jourdain et al., 2020). The initMIP-Antarctica initialization model intercomparison project has demonstrated experiments revealed that ice-sheet ~~models~~ model responses exhibit significant divergence ~~in response~~ due to variations in initial basal melting conditions, with the resulting range accounting for 5 % ~~to~~ 125 % of the total mass change ~~in initialization experiments~~ (Seroussi et al., 2019; ~~Seroussi et al., 2020~~). This pronounced model spread underscores persistent challenges in accurately representing sub-ice-shelf oceanic processes during ice-sheet model initialization (Pritchard et al., 2012; Alevropoulos-Borrill et al., 2020), and may propagate into projection uncertainties, particularly for ice dynamics influenced by oceanic forcing.

~~However, previous~~ Previous model intercomparison projects (e.g., initMIP-Antarctica) combined ice-sheet models with varying numerical complexities and initialization methods (e.g., ~~spin up and data assimilation~~). ~~This diversity makes, making~~ it difficult to ~~explicitly identify the physical mechanisms driving the large range of projection~~ attribute uncertainties ~~to specific sources; our study isolates the impact of oceanic conditions by using a single ice-sheet model with identical initialization except for the basal melting scheme~~. Zhang et al. (2024) addressed this limitation by adopting a single ice-sheet model (Community Ice Sheet Model, CISM; Lipscomb et al., 2019; Berdahl et al., 2023) to investigate the impacts of geothermal heat flux and basal sliding conditions on Greenland Ice Sheet initialization. Extending this approach and considering the crucial role of ice shelves in Antarctica, we propose conducting similar experiments for the Antarctic Ice Sheet (AIS) using ~~the identical a single~~ ice-sheet model and initialization method to assess the impacts of sub-ice-shelf melt rates. This focused investigation will address two key questions: (1) How do varying sub-ice-shelf melt rates impact the model initialization state? (2) How ~~do these melt rates~~ does this initial state affect long-term ~~Antarctic Ice Sheet~~ AIS projections?

Therefore, in this paper, we consider two different sub-ice shelf melt rates ~~approaches-schemes~~ (Section 2) in the ~~ice sheet model~~ (Parallel Ice Sheet Model, PISM) by first spinning-up and then projecting the ~~Antarctica Ice Sheet (AIS)~~.

70 The structure of this paper is organized as follows: Section 2 details the methodological approach and experimental design for projections. Section 3 ~~and presents the key simulation results, while~~ Sections 4 ~~and 5~~ provide comprehensive results and discuss the implications for ice dynamics and sea level rise projections, ~~while Section 5 analyses uncertainties in the model initialization and projection.~~

## 2 Model and Methods

75 We conduct ice-sheet simulations using the Parallel Ice Sheet Model (PISM v.1.0) (Bueler et al., 2007; Martin et al., 2011; Winkelmann et al., 2011; Albrecht et al., 2020), an open-source, three-dimensional thermomechanical coupled model that integrates ice dynamics and thermodynamics. PISM employs a hybrid stress balance strategy (Martin et al., 2011; Winkelmann et al., 2011) by combining the Shallow Ice Approximation (SIA) for grounded ice (Gudmundsson, 2003; Bueler et al., 2007; Pollard & DeConto, 2012) and the Shallow Shelf Approximation (SSA) for floating ice (Hindmarsh, 2006; Bueler & Brown, 2009; Pollard & DeConto, 2012). ~~The grounding-line migration in PISM is optimized through a sub-grid scheme, which interpolates key physical variables such as basal shear stress, basal melt rate, and basal friction based on spatial gradients across the interface between grounded and floating cells (Feldmann et al., 2017; Nowicki et al., 2020). This approach reduces physical gradients across the grounding line and simulates a more realistic and dynamic representation of the ice margin (Leguy et al., 2014; Golledge et al., 2015).~~

85 ~~To keep model consistency and for the convenience of results comparison, we follow the same initialization configuration and initial conditions as in LOW21 but using a different observational sub-ice shelf melt rate obtained from satellite altimetry, radar, and other datasets 2; Table 1).~~ We utilize the BedMachine v.3 dataset (Morlighem et al., 2019) for initial topography, encompassing ice thickness and bedrock topography. Air temperature and precipitation inputs are derived from RACMO 2.3p2, averaged over 1979–2014 (van Wessem et al., 2018). Surface mass balance is calculated using a degree-day model (Ohmura, 2001; Calov & Greve, 2017), with near-surface temperature locally adjusted based on elevation changes using a correction factor of 0.008°C/m (Pittard et al., 2022).

90 The ~~spatial distribution of oceanic conditions in our study is presented in Fig. 1. Based on this data, PISM ocean module provides~~ the sub-ice shelf ~~ice~~ temperature ~~serves and mass flux to the ice dynamics core via two different schemes. Sub-ice shelf temperature is applied as the Dirichlet boundary condition for in the energy conservation, and the code, while~~ sub-ice shelf mass flux ~~enters as a source in the mass conservation equation. In our experiments, the mass flux is represented by derived~~ either ~~an observational directly from observed basal melt rate dataset (our approach, S1) rates~~ or ~~indirectly through a parameterization using ocean temperature and salinity, depending on the available oceanic data. Where directly using observed basal melt rates a parameterized method (LOW21, S2); (Rignot et al., 2013; Fig. 1) and ice-shelf basal temperature (Chambers et al., 2021; Fig. 1), the sub-ice shelf mass flux is computed~~ by Eq. 1:

$$S_1 = \rho_i B, \quad (1)$$

where  $\rho_i$  indicates the ice density, and B represents the sub-ice shelf melt rates. ~~On the other hand, LOW21 employs an ocean model with~~ For simulations driven by Southern Ocean temperature and salinity (Fig. 2, Schmidtke et al.,

2014, Fig. 2)) to calculate the sub-shelf melt as implemented in LOW21 (Lowry et al., 2021), the mass flux is obtained indirectly through a linear thermal forcing (TF-linear) parameterization (Martin et al., 2011), the main calculation equation is as follows) following Eq. 2:

$$S_2 = \rho_{sw} c_m \gamma_T F_{melt} (T_s - T_f) / (L_i \rho_i), \quad (2)$$

where  $\rho_{sw}$  denotes the seawater density,  $c_m$  represents the specific heat capacity of the ocean mixed layer,  $L_i$  refers to the latent heat of phase change for ice,  $\gamma_T$  represents the thermal exchange velocity between seawater and ice (assigned  $\gamma_T = 10^{-4}$ ; Holland and Jenkins, 1999; Hellmer and Olbers, 1989),  $F_{melt}$  is a model parameter (assigned  $F_{melt} = 5 \times 10^{-3}$ , Beckmann and Goosse, 2003),  $T_s$  is the vertically averaged ocean temperature of ocean water between 200 m and 1000 m depth along the continental slope (assigned  $T_s = 271.45$  K, Beckmann and Goosse, 2003; Martin et al., 2011), and  $T_f$  denotes the temperature of seawater at depth  $z_b$  beneath the ice shelf:

$$T_f = 273.15 + 0.0939 - 0.057S_0 + 7.64 \times 10^{-4} z_b, \quad (3)$$

where  $S_0$  denotes the specified ocean salinity (35 psu). During the initialization procedure, to evaluate the specific role of oceanic conditions, we conducted two experiments using PISM: Experiment “S2” replicates the single simulation from LOW21 that used the best-fit parameter set (the one minimizing mismatch with observations), employing a thermodynamic parameterization (Eq. 2) to estimate sub-ice shelf melt rates. Experiment “S1” uses the same model configuration—including all parameters, stress balance approximation, resolution, topography, and atmospheric conditions—but replaces the basal melting scheme with observed basal melt rates derived from satellite altimetry (ICESat-1), radar (OIB and ALOS PALSAR), and model outputs (RACMO2), based on Eq. 1.

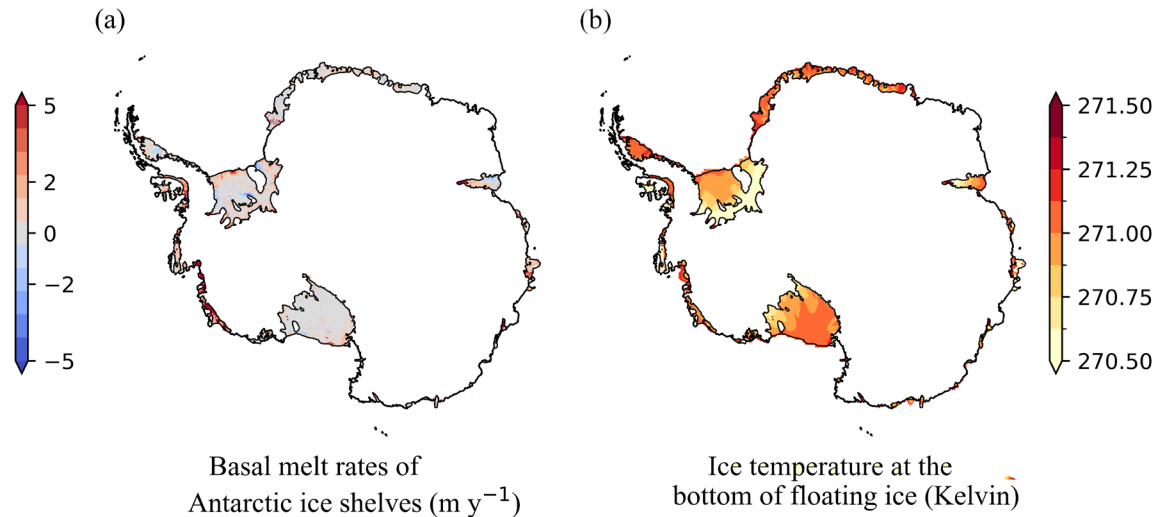


**Figure 1: Ocean conditions used in our simulations S1.** (a) observation of sub-ice shelf basal melt rates (Rignot et al., 2013); (b) Temperature field beneath ice shelves (Chambers et al., 2021).

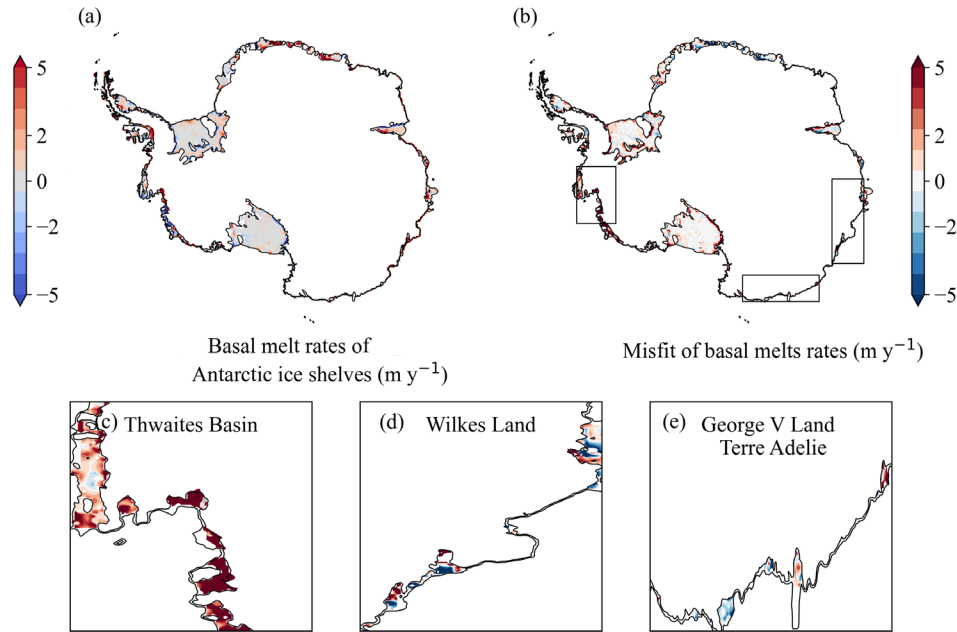


**Figure 2: Comparison of sub-ice shelf melt rates between our study S1 and LOW21 (our study relative to LOW21)-S2.** (a) ~~LOW21 sub~~Sub-ice shelf melt rates derived from ~~ocean model~~the TF-linear parameterization (S2). (b) ~~Differences~~Difference in basal melt rates ~~between our study (Rignot et al., 2013) used in S1 and LOW21-S2~~, with three black boxes highlighting ~~the~~regions of interest: (c) Thwaites Basin, (d) Wilkes Land, and (e) George V Land Terre Adelie.

130 ~~During model initialization, We applied~~ a “multi-stage” spin-up procedure (Golledge et al., 2015; Lowry et al., 2021) ~~is applied~~ to achieve a pseudo-equilibrium ice-sheet state under constant climate conditions, with a 16 km spatial resolution: (1) a brief 10-year smoothing utilizing the shallow ice approximation, (2) a 250,000-year simulation to allow the enthalpy field to reach thermal equilibrium, (3) a 1,500-year ~~evolutionary model run~~ incorporating full model physics, including the application of sub-ice shelf melt rates to constrain ice dynamics, and (4) a 65-year historical run to connect initialization and prediction, during which the current ice ~~sheet~~-thickness is reconstructed. Further, ~~based on the initialized model state and the optimal parameter set from S1, we conduct projection experiments, initiated in from 2015, by employing “high” and “low” scenarios controlled by turning on or off the sub-grid grounding-line scheme in PISM. The “sub-grid scheme on (SGO) scenario” incorporated sub-grid melt interpolation, where “high” utilizes the scheme and “low” omits it near grounding lines, accelerating grounding-line retreat in our~~

140 ~~coarse-resolution model, while the “sub-grid scheme off (SGF) scenario” ignored melt in partially floating cells, yielding more conservative mass loss estimates (Albrecht et al., 2011; Golledge et al., 2015). These experiments used; Nowicki et al., 2020). To ensure that differences in projections originated solely from the model spin-up, we employed the same daily-resolution climate forcing as LOW21 (Lowry et al., 2021), derived from the CMIP5 IPSL-CM5A-MR RCP2.6/8.5 (Barthel et al., 2020; Payne et al., 2021; Nowicki et al., 2021) and the CMIP6 CNRM-CM6-1 SSP1-2.6/5-8.5 product (Nowicki et al., 2016; Kamworapan et al., 2021) 2021; Nowicki et al., 2021) spanning 2015–2100, to~~

145 ~~assess and compare~~ Antarctica's contribution to global mean sea-level rise by 2100. ~~The basal melting scheme was parameterized using the same linear thermodynamic framework for the ice-shelf-ocean boundary layer as that~~

employed in LOW21. This approach explicitly resolves heat and freshwater exchange processes at the ice–ocean interface, driven by oceanic forcing under different RCP/SSP scenarios from 2015 to 2100.

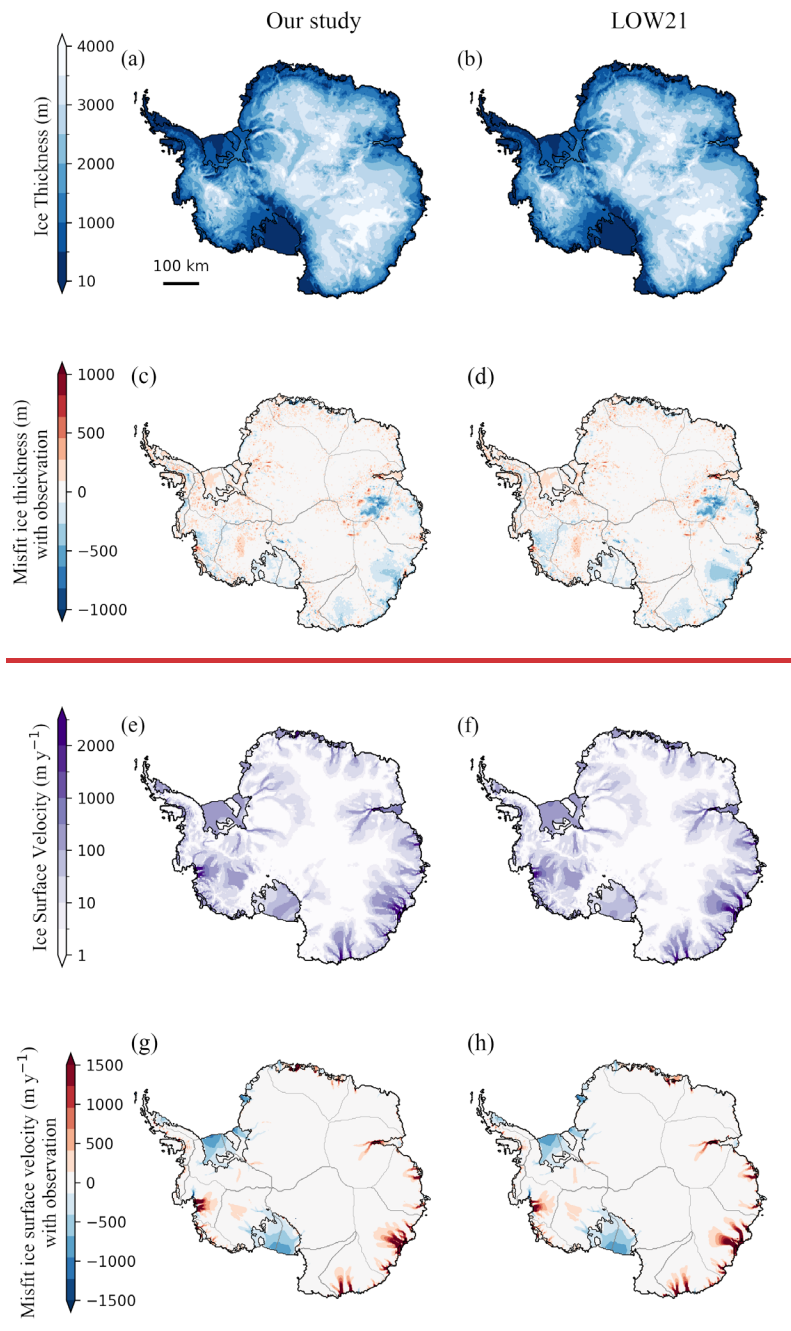
## 150 **3 Model Initialization Results**

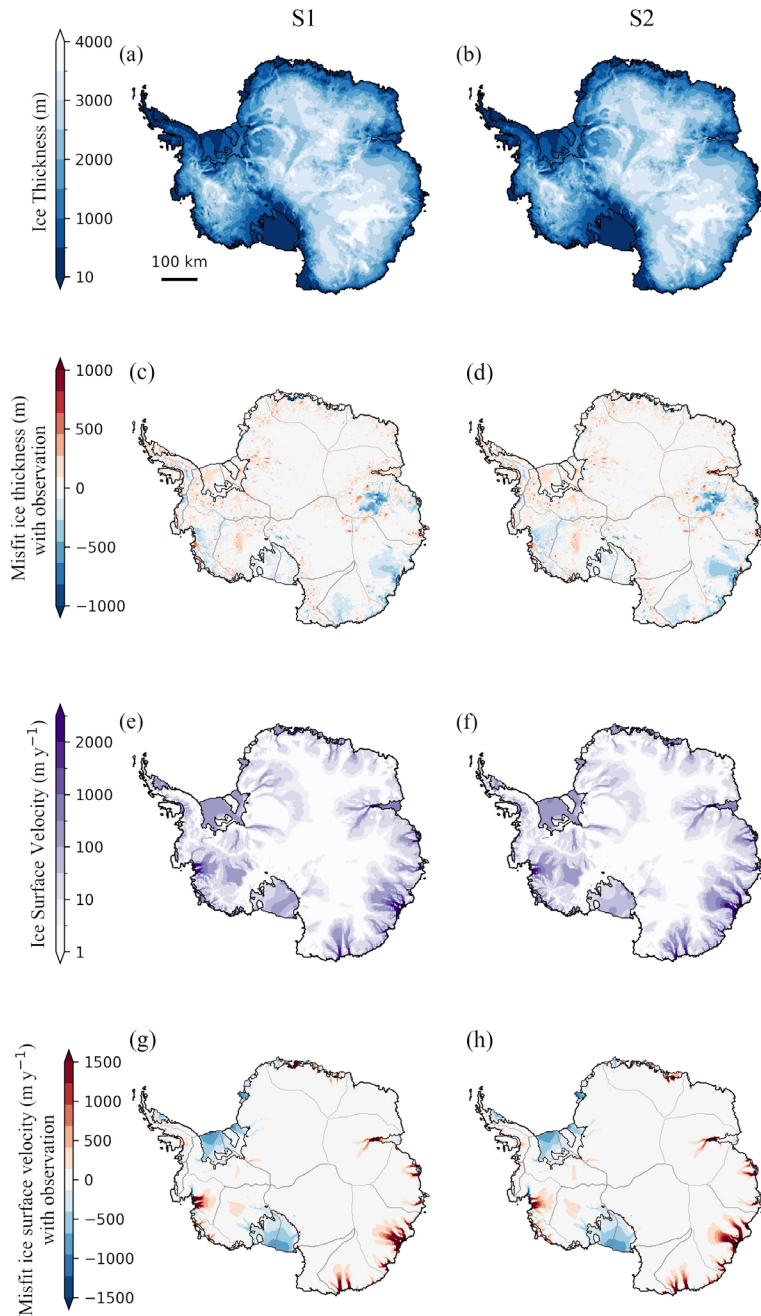
### **3.1 Comparison with the case of different sub-ice shelf melt rates**

We ~~compare our simulations with those of LOW21 in terms of validated the simulated~~ ice thickness and ice surface velocity; results from both S1 and S2 using observational datasets (BedMachine v.3; MEaSUREs Phase-Based Antarctica Ice Velocity Map v.1), ~~with RMSE). The difference of in root mean square error (RMSE) for the two~~ experiments, derived from comparison against observation, is 2 m for ice thickness and 3 m y<sup>-1</sup> for ice surface velocity. Figure 3 shows the differences between model results and observations: the left column displays discrepancies for ~~our S1~~ simulations, while the right column shows those for ~~LOW21 S2~~. The comparison ~~indicates generally consistent~~ shows that the mass distribution and ice flow ~~dynamics of S1 closely match those of S2~~. To better highlight the differences between ~~our simulations and LOW21~~ the two experiments in ice thickness and velocity over Thwaites Glacier, we selected a representative transect (Fig. 7) where discrepancies were most pronounced. Along this transect, we compare the grounding ~~line~~ positions, ice thickness, and surface velocity profiles between ~~our model S1 and LOW21 S2~~.

We also compared ~~our simulations and LOW21~~ the results of two experiments against those from the Antarctica Antarctic ice ~~sheet~~ model initialization ~~results~~ (initMIP-Antarctica) that employed the PISM (Seroussi et al., 2019). Both studies align with ensemble trends in ice mass, ice sheet area, ice shelf area, and potential sea level contributions. ~~Our S1~~ simulations exhibit minor differences in total ice sheet mass (-6% to +11%) and ice area (-7% to -1%) compared to initMIP-Antarctica. Notably, deviations in potential sea level contributions are more pronounced (-17% to -2%), while ice shelf area discrepancies reach 44% relative to the DMI\_PISM simulation (Fig. 4).

Overall, ~~despite while we see~~ minor differences in other metrics between ~~our our two experiments results~~ and ~~that of~~ the initMIP-Antarctica ensemble simulations, ~~both our spinned the spin-up~~ ice volumes (potential sea level contributions) in both S1 ( $25.81 \times 10^6 \text{ km}^3$ ) and ~~the LOW21 S2 experiment~~ ( $25.77 \times 10^6 \text{ km}^3$ ) exhibit close agreement with the observed total ice volume (BedMachine v.3;  $26(\pm 0.4) \times 10^6 \text{ km}^3$ ). This validates the robustness of our initialization configuration and lends us confidence for future projection experiments.





175

**Figure 3: Comparing ~~our simulation (left column) and LOW21 (right column) relative to simulated initial state with observations.~~ Modeled ice thickness (m) and surface ice velocity ( $\text{m y}^{-1}$ ) at the end of spin-up. The left column shows ice thickness and ice surface velocity results from S1, alongside their difference from observation (Morlighem et al., 2019; Mouginot et al., 2019). The right column shows the corresponding results from S2, sharing common color bars with S1.**

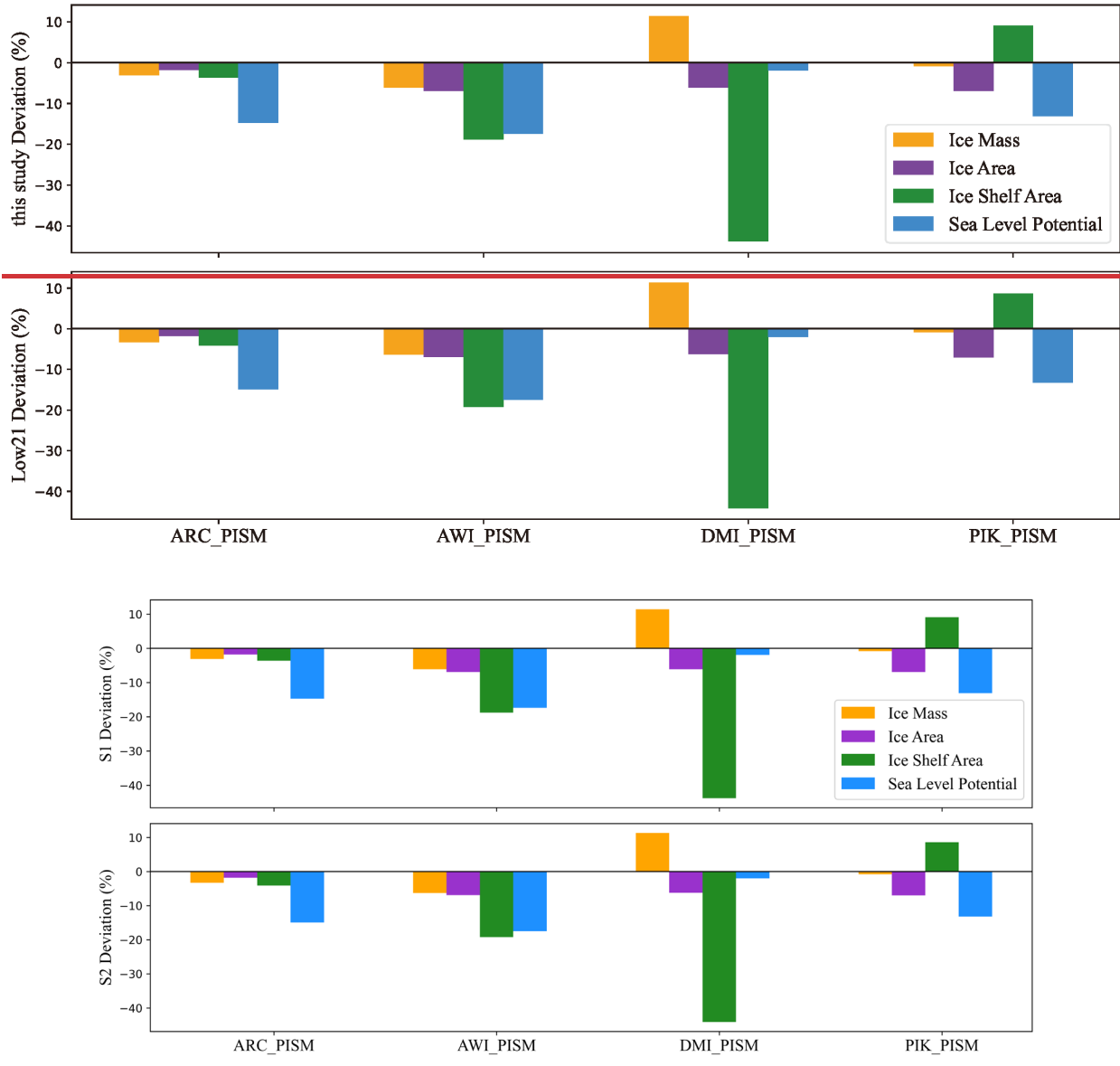


Figure 4: Percentage deviations in steady-state metrics (ice mass, ice sheet area, ice shelf area, potential sea level contribution) relative to the initMIP-Antarctica PISM-based ensemble (Seroussi et al., 2019). The vertical axis represents the percentage deviation between the results of our study, LOW21+S1, S2, and the simulations from participating institutions (\*\_PISM, where \* denotes the institution abbreviation).

185

### 3.2 Differences in Marine Ice-Sheet Regions-sheet regions

As clearly can be seen in Fig. 5, there are significant velocity differences in three marine-based regions characterized by retrograde bed slopes: (Fig. 5): Thwaites Basin (TB) in the West Antarctica (WAIS), Wilkes Land (WL), and George V Land–Terre Adelie (GVL) in the East Antarctica (EAIS). These regions are particularly susceptible to MISI due to their subglacial topography (Joughin et al., 2014; Mengel & Levermann, 2014; Greenbaum et al., 2015).

190

In the Thwaites Basin, the observed sub-ice shelf melt rates (used in S1 (reaching 17.7 m y<sup>-1</sup> beneath Thwaites ice shelf, Fig. 1)) ~~accelerate exceed S2's parameterized values by approximately 5 m y<sup>-1</sup> (Fig. 2). This higher basal melting weakens the ice-surface-velocity-downstream-shelf buttressing effect and accelerates the grounded ice flow,~~ with a corresponding 74 m y<sup>-1</sup> RMSE difference from LOW2+S2 (Fig. 5f). Compared to S2, this results in~~This led to~~ around 40 m more ice thinning near the grounding line and an approximately 30 km more grounding-line retreat (Fig. 7), ~~compared to the case in LOW21, demonstrating an intrinsic connection within the ice-sheet system. This systemic response is further evidenced by widespread thickening while most upstream, areas exhibit positive thickness with a anomalies (mean anomaly of 49.5 m), suggesting complex feedback in ice dynamics.~~ The ice volume above flotation ~~in TB in our study S1~~ shows a 5.5-fold bias reduction (-0.59%, 1.19 m SLE) compared to LOW2+S2 (-3.28%, 1.16 m SLE), aligning closely with observations (1.20 ± 0.02 m SLE, Table 1).

In the Wilkes Land, the ~~Totten~~Totten Glacier exhibits increased ice surface-velocity~~flow~~ under observed melt rates, yielding a 44 m y<sup>-1</sup> lower RMSE in our study S1 relative to LOW2+S2 (Fig. 5g), leading to regional mean ice thinning of 38.5 m. ~~This generates stronger~~The faster flow of Totten Glacier strengthens lateral resistance ~~for~~along its boundaries with adjacent glaciers, subsequently reducing ice ~~flow in glaciers upstream of flux into~~ the Voyeykov and Moscow Ice Shelves, ~~exhibiting a~~ (Gagliardini et al., 2010; Van Der Veen et al., 2014). This dynamic response is consistent with the simulated mean thickness anomaly of +39.2 m across these regions. The ice volume above flotation bias in WL ~~decreased~~decreases to -4.61% (6.63 m SLE) in our S1 results, compared to -5.14% (6.59 m SLE) in LOW2+S2, achieving a 10% improvement relative to the observed 6.95 ± 0.09 m SLE (Table 1).

In the George V Land–Terre Adelie, the enhanced flow of the Ninnis Ice Shelf in S1 results in increased ice discharge and regional mean thinning (33.7 m). Conversely, the Cook and Mertz Ice Shelves and their upstream glaciers experience reduced ice flux, causing regional ice thickness to increase by 25.5 m on average relative to LOW21. ~~Our S2. S1~~ simulations demonstrate a reduced ice volume above flotation bias of -5.23% (3.35 m SLE) in WL, outperforming LOW21's -5.42% (3.34 m SLE) of S2 and reflecting closer agreement with the observed 3.53 ± 0.04 m SLE (Table 1).

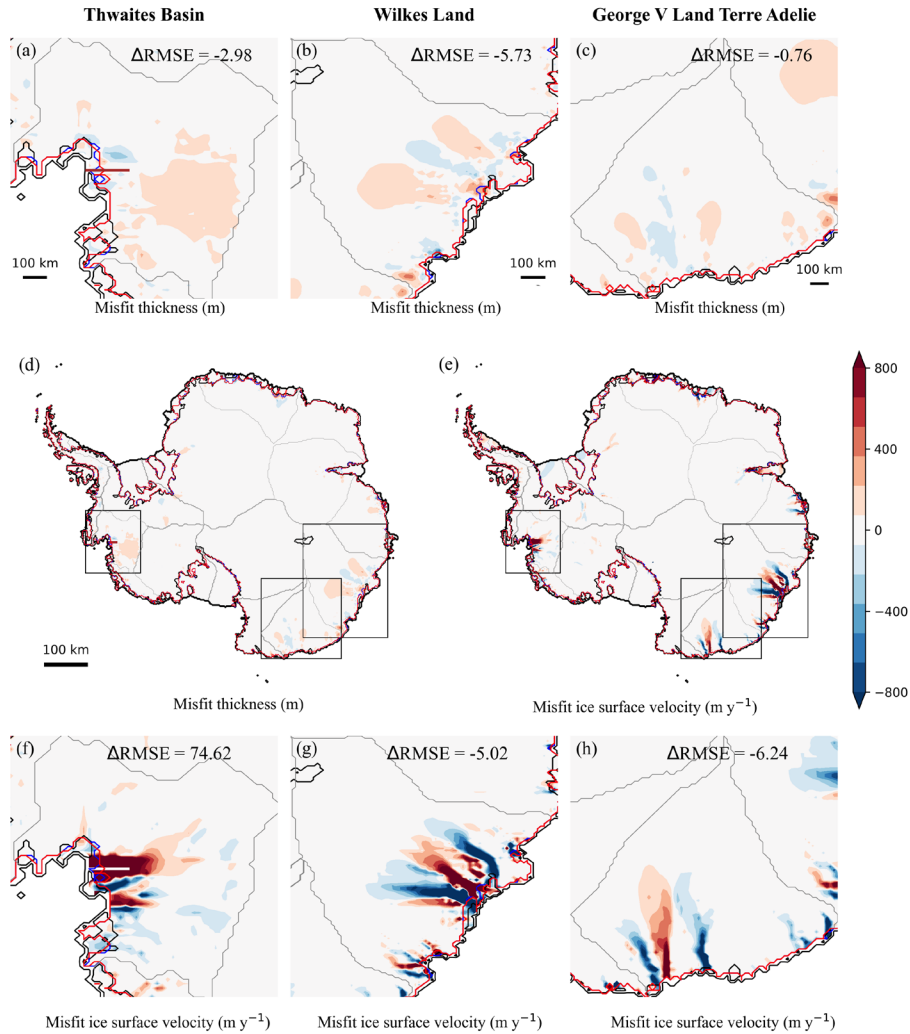


**Figure 5: Comparison of ~~spin-up~~ ice thickness and velocity misfits between ~~our results~~S1 and LOW21 (our study relative to LOW21) S2.** (a–c) Ice thickness differences (S1 relative to S2) in the TB, WL, and GVL, respectively. (f–h) Ice surface velocity misfits in the TB, WL, and GVL, respectively. The difference in root mean square error ( $\Delta\text{RMSE} = \text{RMSE}_{s1} - \text{RMSE}_{s2}$ ) between ~~our results~~S1 and LOW21 S2, compared to observations ( $\Delta\text{RMSE} = \text{RMSE}_{s1} - \text{RMSE}_{s2}$ ). (d) and (e) present the deviations in ice thickness and surface velocity (our study relative to LOW21) between the two simulation experiments, with three black boxes highlighting regions showing the most significant discrepancies. Grounding lines: LOW21 S2 (blue), our study S1 (red), and observed data (black) from BedMachine v.3 (Morlighem et al., 2019). The profile line locations corresponding to Fig. 7 are in Thwaites Glacier: (a), (d) brown; (f) white.

220

225

A comparison of simulation results between ~~our study~~S1 and LOW21 S2 for three marine ice sheet basins (TB, WL, and GVL; Table 1) reveals that the ice-sheet model driven by observed sub-ice shelf melt rates achieves slightly better alignment with observations. Although the RMSE of ice surface velocity ~~increases~~ (in the TB shows an increase of  $74 \text{ m y}^{-1}$  in the TBS1 compared to LOW21 S2 (Fig. 5f), the ~~overall bias in~~ ice volume ~~bias above flotation~~ decreases by ~~approximately 2.8%~~, while ~~volumethe~~ biases for WL and GVL ~~are~~ reduced by 0.5% and 0.2% (Table 1), respectively.

230 **Table 1:** Ice volume above flotation (m SLE) in three marine ice sheet basins, ~~simulated at 16 km resolution after spin-up, simulated~~  
~~at 16 km resolution. “S1” denotes the experiment using observed basal melt rates based on Eq. 1, while “S2” refers to the simulation~~  
~~that replicates LOW21 using the thermodynamic parameterization in Eq. 2.~~

Basins	Observation	<del>Our</del> <del>study</del> S1	Misfit	<del>LOW21</del> S2	Misfit
Thwaites Basin (TB)	1.20 ( $\pm 0.02$ )	1.19	-0.59%	1.16	-3.28%
Wilkes Land (WL)	6.95 ( $\pm 0.09$ )	6.63	-4.61%	6.59	-5.14%
George V Land Terre Adelie (GVL)	3.53 ( $\pm 0.04$ )	3.35	-5.23%	3.34	-5.42%

### 3.3 Marine Ice Sheet dynamics during model spin-up

235 In the WAIS, particularly for glaciers adjacent to the Amundsen Sea Embayment, the subglacial bedrock topography  
lying below sea level amplifies the sensitivity to ocean-driven forcings (Pritchard et al., 2012). Previous studies stated  
that the Aurora Subglacial Basin in WL and the Wilkes Subglacial Basin in GVL, in the EAIS, are characterized by  
extensive sedimentary basins that are highly susceptible to warming ocean conditions (Aitken et al., 2014; Frederick  
et al., 2016; Noble et al., 2020). These basins are also subject to an active subglacial hydrology process (Wright et al.,  
2012), and evidence of ocean-driven dynamic ice loss has been documented along the ice-sheet margin (Li et al.,  
240 2016). The interplay between oceanic forcing, subglacial hydrology, and sedimentary geology significantly influences  
ice-sheet dynamics in these regions.

In the S1 experiment~~this study, the application of observed basal melt rates with~~ enhanced oceanic forcing (Fig. 2),  
~~which is represented by higher basal melt rates,~~ intensifies ice-shelf basal melting, leading to geometric thinning and  
reduced buttressing effect of upstream ice flow (Gudmundsson, 2013; Miles et al., 2022). This triggers grounding-  
245 line retreat, ~~which accelerat~~~~ing ice velocity. Accelerated~~ ice flow, ~~substantially~~ amplifies strain rates, ~~and leading to~~  
enhanced ~~d~~ dissipative heating (Cuffey & Paterson, 2010; Dawson et al., 2022), ~~and therefore~~~~thereby~~ increasing  
temperatures at the basal ice layer (Fig. 6a-c). It then promotes basal melting (Fig. 6d-f) while reducing ice viscosity  
via thermal softening, collectively facilitating enhanced deformation and potentially increasing ice-sheet  
destabilization (Hindmarsh, 2006; Adams et al., 2021). Additionally, subglacial meltwater lubricates the ice-bed  
250 interface, reducing basal friction through decreased effective pressure and accelerating ice flow (Fig. 6g-l). Enhanced  
sliding generates additional strain heating (Garbe et al., 2020), which promotes further basal melting and meltwater  
production. ~~This~~In this positive feedback process ~~—where, termed the basal thermal-hydrological feedback,~~ elevated  
basal water ~~content~~content persistently reduces resistance ~~to ice motion (Zhao et al., 2025) — is termed the basal~~  
~~thermal hydrological feedback, thereby facilitating ice sliding and ultimately leading to ice thinning~~ (Fowler et al.,  
255 2001; Clarke, 2005; van Pelt & Oleremans, 2012; Zhao et al., 2025), ~~facilitating the speed of ice sliding and~~  
~~ultimately leading to ice thinning.~~

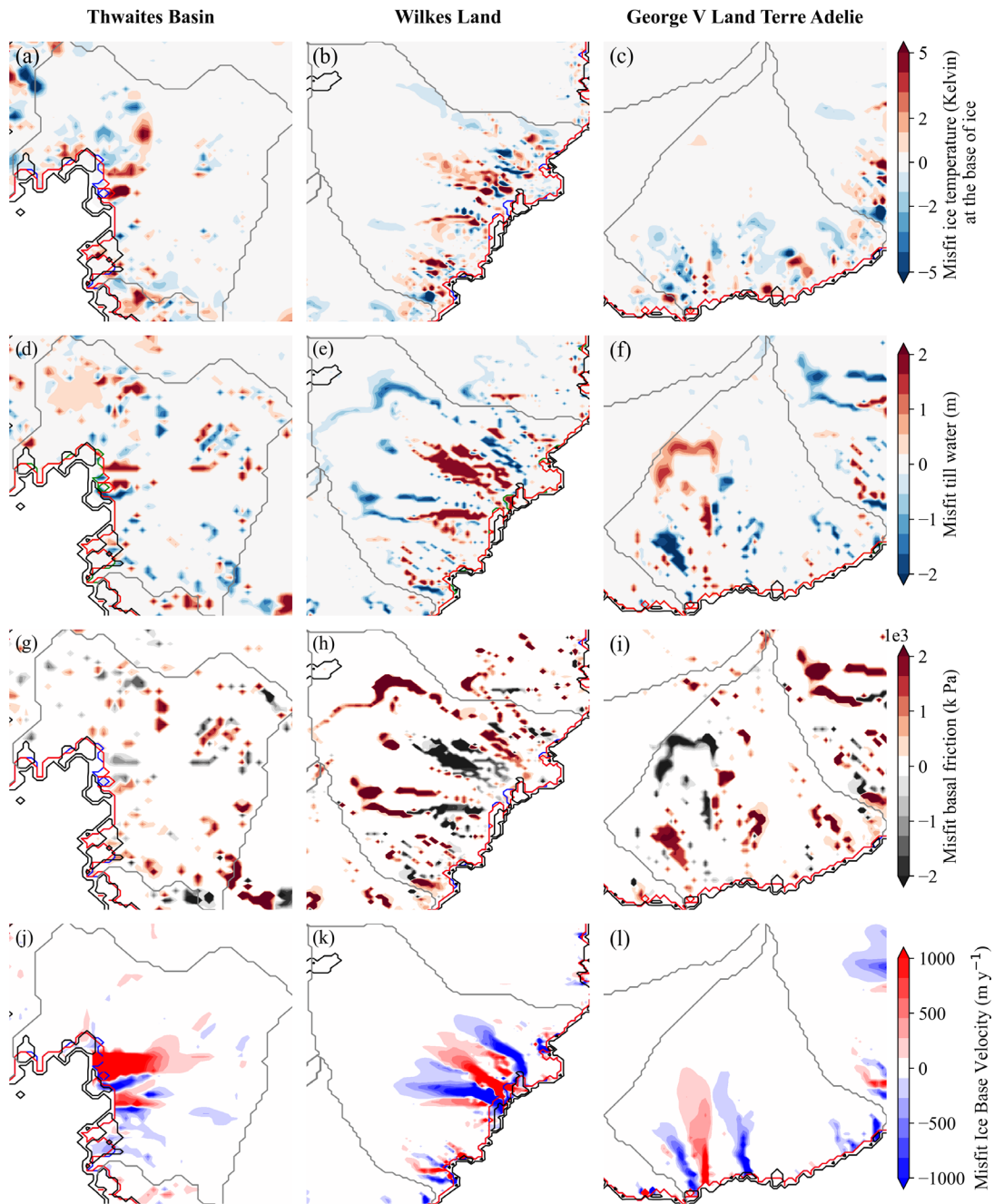


Figure 6: Spatial distribution of misfits ([our-studyS1](#) relative to [LOW21S2](#)) in basal ice temperature field (Kelvin) (a-c), basal till water content (m) (d-f), basal friction (k Pa) (g-i), and basal velocity ( $\text{m y}^{-1}$ ) (j-l) in the three basins. The blue and red lines indicate the grounding-line positions for [LOW21S2](#) and [our-studyS1](#), respectively, while the black line represents the observed grounding line from BedMachine v.3.

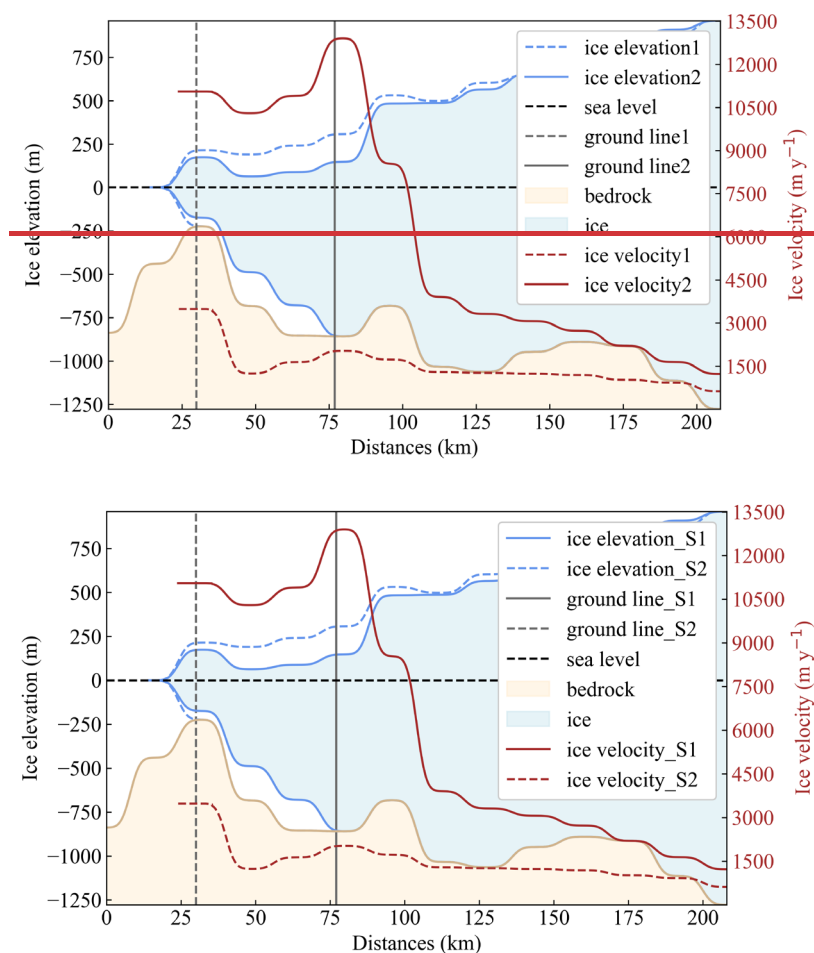
### 3.4 Grounding line location comparison

The impact of sub-ice shelf melt rates on ice-sheet initialization can also be seen at the locations of the grounding line. Particularly, in [the](#) WAIS, the retrograde bed topography amplifies [the](#) susceptibility to MISI (Pritchard et al.,

265 2012; Ritz et al., 2015), rendering it highly responsive to ocean forcing. ~~The observed sub-ice shelf melt rates applied in our simulations exceed LOW21's parameterized values by roughly 5 m yr<sup>-1</sup> beneath Thwaites and Pine Island ice shelves (Fig. 2).~~ During spin-up, these elevated basal melt rates (Fig. 2) trigger MISI more easily, causing the grounding line on retrograde bedrock to retreat continuously until reaching a new steady state (Rignot et al., 2019; Li et al., 2022). Cross-sectional analysis of Thwaites Glacier (Fig. 7) demonstrates this mechanism, with enhanced basal melting, causing an approximately 30 km grounding-line retreat from its stabilized position (~~LOW21, purple S2, dashed grey line in Fig. 7~~) to a new quasi-stable state (~~our study, orange S1, solid grey line in Fig. 7~~). ~~This retreat in S1 increases ice discharge due to the reduced ice-shelf buttressing effect, resulting in roughly 40 m ice thinning proximal to the grounding line and an anomalous nearly twofold acceleration in ice surface velocity compared to the LOW21 S2 results.~~ This feedback highlights how ocean-forced basal melting propagates through ice-sheet dynamics processes to alter initial ice geometry.

270

275



280 **Figure 7: Comparison between our simulation S1 and LOW21 S2 along the Thwaites Basin transect: after spin-up.** Ice elevation (blue line), ice surface velocity (brown line), and grounding-line positions (grey line) for S1 and S2 are indicated by the grey solid and dashed lines distinguished by 1 and 2, based on LOW21 and our study, respectively. Sea level: black dashed line. In fact, the retreat of the grounding-line position varies across different ice streams, influenced by factors such as basin size, water depth, bed roughness, neighboring depending on topography, neighbouring ice shelf basal melt rates,

and ice velocities (Martin et al., 2011; Pittard et al., 2022). Consequently, the discrepancies between observed and simulated grounding-line positions differ across various regions of the AIS. For instance, the grounding line of the Siple Coast on the west side of the Ross Ice Shelf in our simulation S1 agrees with LOW21 S2 but extends further to the nearshore compared to the observation (Fig. 5d-e). This discrepancy can be attributed likely arises from a self-limiting, stabilizing mechanism inherent to prograde slopes. As the reversibility of grounding-line migration on a retrograde slope retreats into shallower bedrock, which is characterized by oscillatory the ice thins and ice flux decreases; this leads to ice re-accumulation that prompts grounding-line readvancement, creating reversible shifts (Martin around an equilibrium point (Huybers et al., 2017) 2011; Pattyn et al., 2012). Notably, under a consistent model parameter configuration, the inclusion of observed sub-ice shelf melt rates did not significantly alter the steady-state grounding-line migration position across the whole AIS, except within three marine-based regions.

## 4 Model Projection Results

### 4.1 Global mean sea level contribution from AIS

Prognostic simulations from (2015 to 2100 revealed) show that the divergent initial ice mass changes compared to LOW21, particularly in WAIS. Under various climate scenarios, our model projected AIS sheet states of S1 and S2 lead to markedly different sea-level contributions to sea level rise ranging from across the AIS, even under identical climatic forcings and basal melting scheme (Figs. 8, 9). Specifically, S1-based projections of a 0.20 to 0.52 m SLE (Fig. 8), compared to total AIS contribution exceed the 0 to 0.32 m SLE in LOW21—an average increase of range of the LOW21 ensemble projections (which includes predicted results from S2) by roughly 0.18 m SLE (—, representing a ~57% increase (Fig. 8). This discrepancy is driven primarily by enhanced ice loss from the West Antarctica (0.29–0.34 m SLE, Table 2), where high sub-ice shelf melt rates triggered MISI more readily, whereas the East Antarctica and the Antarctic Peninsula (AP) show minimal sea level contributions by 2100, i.e., 0.01–0.02 m SLE and 0.0011–0.0045 m SLE, respectively (Table 2). However, the S1-based projections of Antarctic ice sheet AIS contributions to sea-level rise from 2015 to 2075 exhibit no significant dependence on emission scenarios, with substantial overlap in prediction ranges (Fig. 8c),—, which This is relative to consistent with the hysteretic response of ice-sheet dynamics to climate, meaning that the ice sheet's state in the near-term (2015-2075) is largely determined by historical forcing, masking the influence of divergent future scenarios (Garbe et al., 2020).

The SSP scenarios simulate higher warming magnitudes (averaging +0.14–0.25 °C) than RCP scenarios at equivalent radiative forcing levels (Tokarska et al., 2020; Wyser et al., 2020; Rounce et al., 2023), driving substantial divergences in AIS projections. By 2100, the mean AIS contributions to sea-level rise based on S1 under SSP 5-8.5 reach 0.36 m SLE—12.5% higher than the RCP 8.5 equivalent (0.32 m SLE)—with RCP high-emission projections even matching SSP low-scenario results (Fig. 8d, Table 2). Based on 2100 trajectory extensions, persistent ice mass is projected through the early 22nd century under These differences between RCP 8.5 and SSP 5-8.5 projections are largely due to the SSP scenarios, whereas in CMIP6 climate models simulating higher warming magnitudes (averaging +0.14–0.25 °C) than RCP scenarios in CMIP5 at equivalent radiative forcing (Tokarska et al., 2020; Wyser et al., 2020; Rounce et al., 2023), based RCP simulations indicate stabilizing ice mass trends beyond 2100. Consequently, under

anthropogenic warming, ~~Antarctic contributions to the~~ sea-level ~~rise in commitment of AIS under~~ SSP high-risk scenarios ~~demand demands~~ heightened scientific attention ~~due to amplified ice-climate feedback.~~

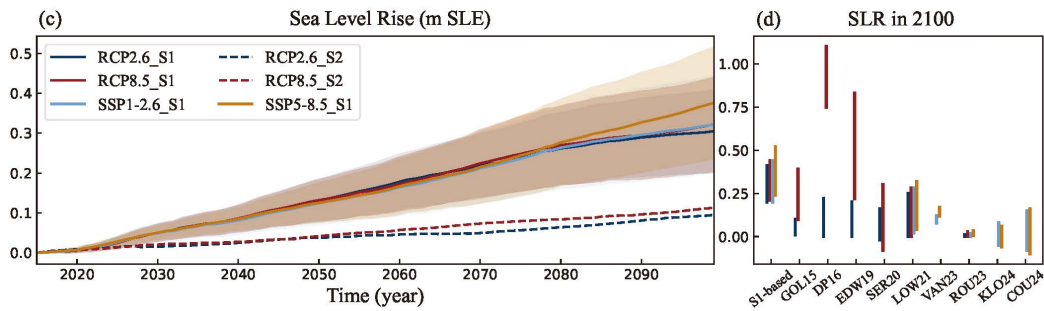
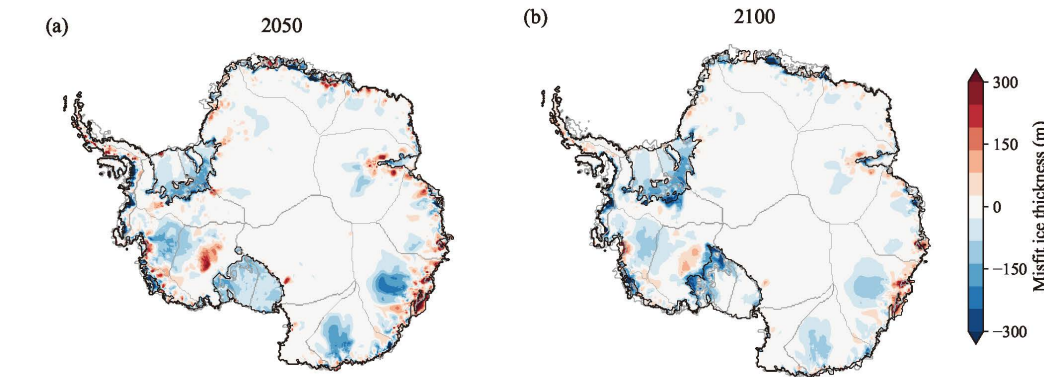
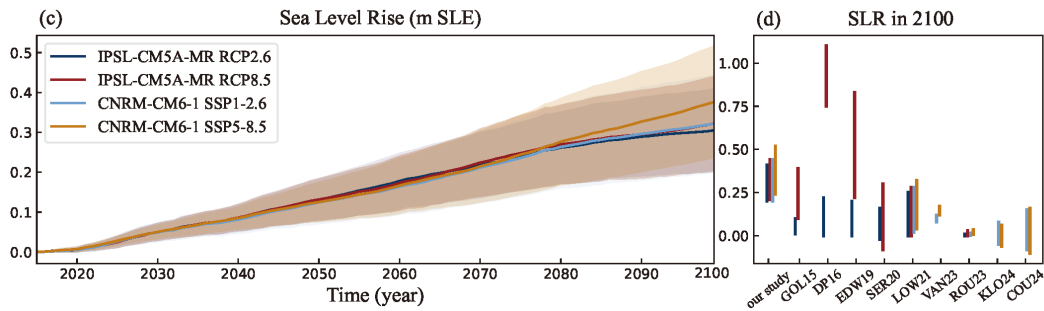
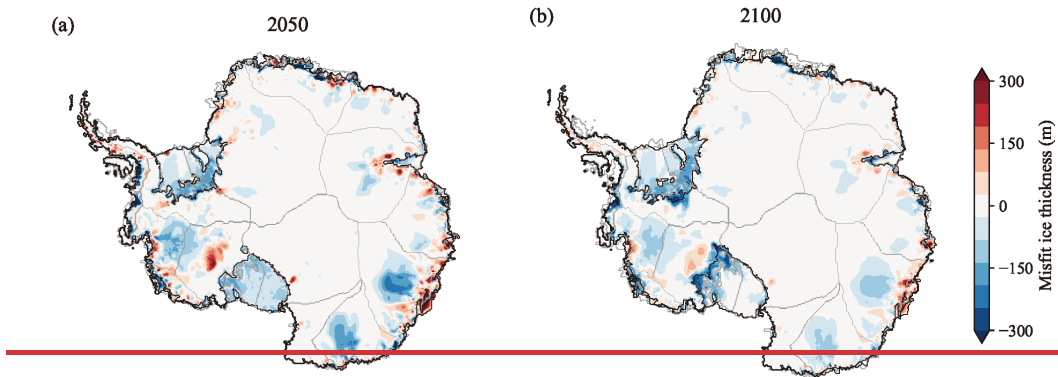


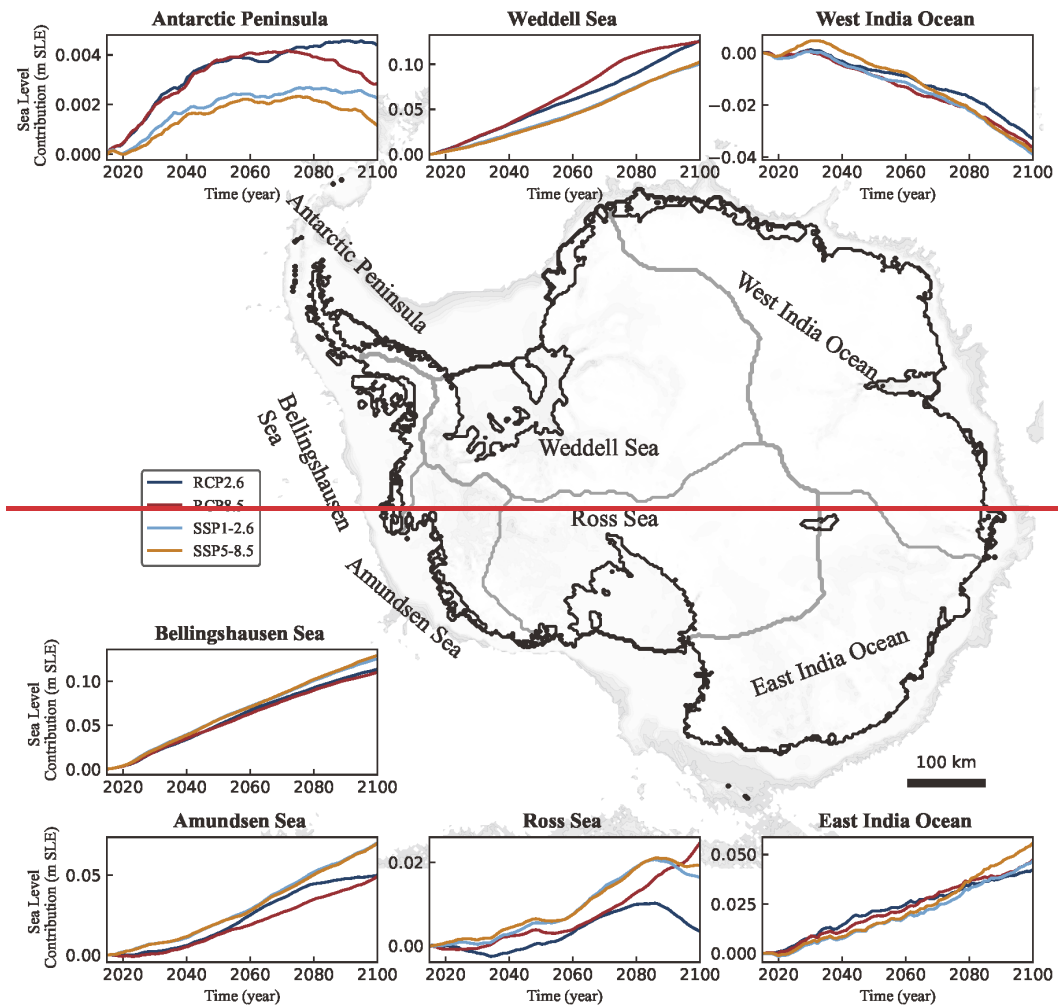
**Figure 8: Ice sheet thickness misfits and projected contribution of the AIS to sea-level rise (m SLE).** ~~Mean Spatial differences in the projected mean ice thickness spatial differences (our study relative to LOW21) between the multi-scenario (RCP 2.6 and RCP 8.5) ensemble means based on S1 and S2 in 2050 (a) and 2100 (b), under RCP scenarios. (c) Predicted sea level rise from “high” and “low” for “SGO scenario” to “SGF scenario” simulations under four scenarios (color shading) and mean values (color lines). The dashed lines represent projections from the S2 initial state—a set of results from the LOW21 ensemble projections: red for RCP 8.5, blue for RCP 2.6. (d) Comparison of p~~Projected contributions to sea-level rise (SLR) by 2100 based on S1, between our study and compared to other studies: CHU13 (Church et al., 2013), GOL15 (Golledge et al., 2015), DP16 (DeConto & Pollard, 2016), EDW19 (Edwards et al., 2019), SER20 (Seroussi et al., 2020), LOW21 (Lowry et al., 2021), VAN23 (van der Linden et al., 2023), KLO24 (Klose et al., 2024), and COU24 (Coulon et al., 2024).

## 4.2 Regional Contributions to Global Mean Sea Level Rise

To explore the spatially variable response of the AIS, we partitioned the ice sheet into seven sectors based on their adjacency to surrounding oceans (Fig. 9). Following the IMBIE (Zwally et al., 2012), we further subdivided the East Antarctica into the East Indian Ocean (EIO) and West Indian Ocean (WIO) sectors. This regional breakdown reveals stark contrasts in the mechanisms and magnitudes of sea level rise across the WAIS, EAIS, and AP (Fig. 9, Table 2), highlighting their distinct sensitivities to climate forcings. The WAIS emerges as the primary driver of AIS-related sea level rise, contributing 0.29–0.34 m SLE by 2100. ~~This significant~~A mechanism similar to that observed in recent decades may be responsible for the projected mass loss ~~is propelled by. Specifically,~~ anthropogenic greenhouse gas emissions, which have significantly altered warming could alter shelf-break wind patterns over the Amundsen and Bellingshausen Seas (AS/BS) embayments (Holland et al., 2019; Noble et al., 2020). ~~These altered winds facilitate,~~ potentially facilitating greater intrusion of warm Circumpolar Deep Water onto the continental shelf, water and intensifying basal ice melting beneath ice shelves (Dinniman et al., 2016; Noble et al., 2020; Li et al., 2023). ~~The resultant thinning diminishes ice~~The resulting reduction in ice-shelf buttressing, ~~accelerating the~~ accelerates ice discharge, which explains the dominance of grounded ice, particularly from the Amundsen Sea (AS) and Bellingshausen Sea (BS) Embayment. Our simulations suggest that the mass loss of these the AS and BS sectors accounts for roughly —accounting for ~55% of total WAIS mass loss in our projections (Table 2). ~~’s total contribution (Table 2), highlighting their critical influence on future sea level trends.~~

The EAIS presents a more complex picture, with a net contribution of 0.01–0.02 m SLE by 2100. While the integrated signal is small, it masks pronounced regional heterogeneity in mass changes. The net mass gain in the West Indian Ocean (WIO) sector ~~presents~~shown in the S1-based projection may be linked to enhanced moisture transport from the Southern Ocean, a net mass gain, mechanism consistent with observational trends (Boening et al., 2012) ~~because enhanced moisture transport from the Southern Ocean drives~~that would promote increased ice surface accumulation. ~~This~~However, this marginal gain, however, is counteracted by ice dynamical adjustments within the East Indian Ocean (EIO) sector, specifically across the WL, where enhanced oceanic thermal forcing drives accelerated ice mass loss from the dynamically vulnerable Totten Glacier (Konrad et al., 2018). This contrast between surface mass balance gains and ice—dynamic losses underscores the spatially heterogeneous response of EAIS, modulated by regional bathymetry and ocean-driven melt.

The AP plays a comparatively minor role in sea level rise, with contributions ranging from 0.0011–0.0043 m SLE by 2100. Peak mass loss occurs between 2075 and 2079, reaching 0.0061 m SLE under RCP 8.5 and 0.0045 m SLE under SSP 5-8.5, followed by a gradual decline (Fig. 9). ~~This transient pattern is tied to the intensification of polar westerly winds, which could enhanced snowfall in the northern AP, which may partially offset warming-induced ice discharge by enhancing snowfall in the northern AP, thus creating and thus generate~~ a negative feedback mechanism that suppresses AIS mass loss (Goodwin et al., 2016). Given its limited ice volume, however, the AP’s overall impact on sea level rise remains marginal. The findings underscore the divergent climate responses of the EAIS, AP, and the WAIS. While the EAIS and AP exhibit mass gain or loss depending on the balance between accumulation and ablation, the WAIS is primarily driven by dynamic mass loss resulting from changes in oceanographic conditions.



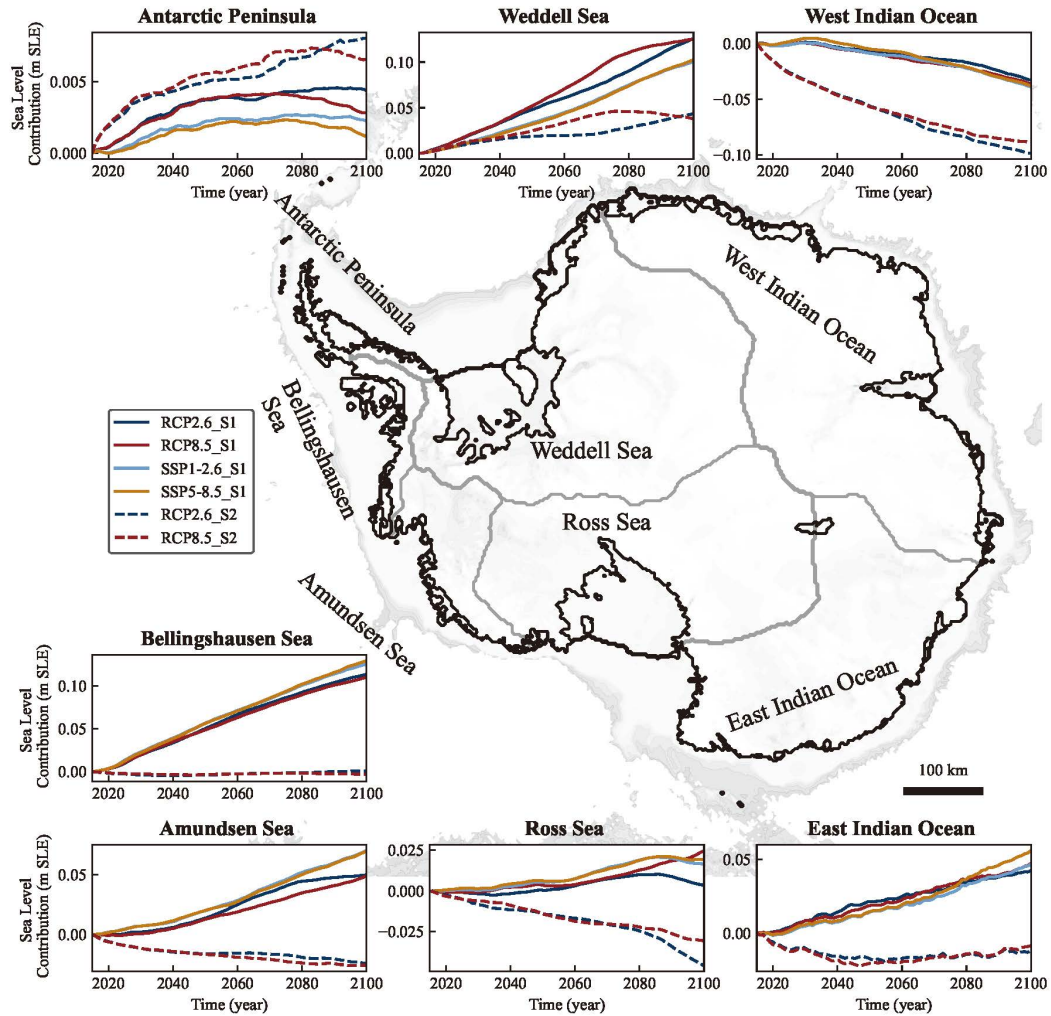


Figure 9: The mean contribution of the AIS seven sectors of AIS to sea level rise (m SLE) from 2015 to 2100. Colored (m SLE). The solid and dashed lines correspond to represent projections from the S1 and S2 initial states, respectively, under different climate scenarios, with the S2 predicted results being part of the LOW21 ensemble projections (red for RCP 8.5, blue for RCP 2.6).

Table 2: Sea level contribution (m SLE) of Antarctic Ice Sheet Basins by 2100. The confidence intervals represent the range of sea-level contribution from the “SGO scenario” to the “SGF scenario” simulation across different RCP/SSP scenarios; the single value denotes the mean value of this range.

Region	RCP 2.6	RCP 8.5	SSP 1-2.6	SSP 5-8.5
Bellingshausen Sea (BS)	0.1138 (0.0857, 0.1419)	0.1102 (0.0813, 0.1391)	0.1256 (0.0982, 0.1530)	0.1297 (0.1064, 0.1585)
Amundsen Sea (AS)	0.0499 (0.0405, 0.0593)	0.0493 (0.0386, 0.0599)	0.0701 (0.0553, 0.0850)	0.0700 (0.0548, 0.0968)
Ross Sea (RS)	0.0034 (-0.0089, 0.0157)	0.0247 (-0.0009, 0.0503)	0.0163 (-0.0107, 0.0435)	0.0193 (-0.0048, 0.0552)
Weddell Sea (WS)	0.1260	0.1249	0.1005	0.1025

	(0.0759, 0.1762)	(0.0734, 0.1764)	(0.0542, 0.1467)	(0.0582, 0.1638)
<u>The West Antarctica Ice Sheet</u> (WAIS)	0.2931 (0.1932, 0.3931)	0.3090 (0.1924, 0.4257)	0.3126 (0.197, 0.4282)	0.3444 (0.2146, 0.4743)
West <u>India</u> Indian Ocean (WIO)	-0.0330 (-0.0448, -0.0211)	-0.0363 (-0.0560, -0.0166)	-0.0389 (-0.0531, -0.0247)	-0.0379 (-0.0471, -0.0227)
East <u>India</u> Indian Ocean (EIO)	0.0423 (0.0269, 0.0578)	0.0473 (0.0277, 0.0669)	0.0467 (0.0284, 0.0650)	0.0559 (0.0467, 0.0867)
<u>The East Antarctica Ice Sheet</u> (EAIS)	0.0093 (0.0058, 0.0130)	0.0110 (0.0109, 0.0111)	0.0078 (0.0037, 0.0119)	0.0180 (0.0240, 0.0396)
Antarctica Peninsula (AP)	0.0043 (0.0024, 0.0062)	0.0028 (0.0007, 0.0049)	0.0022 (0.00004, 0.0044)	0.0011 (-0.0021, 0.0034)
<u>Antarctica Ice Sheet</u> (AIS)	0.3067 (0.2014, 0.4123)	0.3228 (0.2042, 0.4415)	0.3226 (0.2007, 0.4445)	0.3635 (0.2365, 0.5173)

### 4.3 Comparison with previous projections

Our projections of the S1-based simulation projects AIS contributions to sea level rise by 2100 under the SSP 5-8.5 scenario diverge significantly from previous estimates, particularly for the WAIS. While ensemble projections from the The Coupled Model Intercomparison Project Phase 6 models (CMIP6, Edwards et al., 2021) employed Gaussian process emulators—statistical approximations built upon ice-sheet simulations for ISMIP6 (Nowicki et al., 2016, 2020) and GlacierMIP Phase 2 (Hock et al., 2019)—to generate sea-level projections. While their ensemble projections suggest that the WAIS contributions range from -0.04 to 0.11 m SLE, our study S1-based projections show predicts a significantly higher contribution of 0.20–0.47 m SLE. For the EAIS and AP, our S1-derived projected sea level contributions (0.03–0.04 m SLE and -0.0021–0.0034 m SLE, respectively; Table 2) align closely with the emulator results (-0.05–0.06 m SLE and -0.01–0.02 m SLE, respectively), with the WAIS emerging as the dominant divergence source.

Compared to the full ensemble results of ISMIP6 (Ice Sheet Model Intercomparison for CMIP6) Antarctic projections under RCP 8.5 (Seroussi et al., 2020), our WAIS the S1-based projected sea-level contribution exceeds it by for the WAIS is approximately 0.15 m SLE, with higher, while the AP shows shows a slight increase (~0.002 m SLE), and the EAIS exhibiting exhibits a minor reduction (~0.02 m SLE). The ISMIP6-Antarctica projections improve a more comprehensive representation of potential Antarctic sea-level contribution under climatic forcings, with the parameterizations of oceanic conditions into basal melt rates being the dominant source of uncertainty (Seroussi et al., 2020). However, these experiments cannot identify the specific physical mechanisms behind the inter-model differences. Although a key limitation of our single model experiment is its reliance on PISM-specific parameterizations, which restrict the range of projected sea-level contributions and provide limited statistical uncertainty. Nevertheless, by comparing observed and parameterized basal melt rates as represented in model

simulations under a consistent single-model framework, our experiments identify the specific regions and dynamic mechanisms underlying the ISMIP6 projection uncertainty associated with the representation of oceanic conditions.

400 These results demonstrate significant deviations in the WAIS sea-level contributions compared to prior studies projections, consistently aligning with the predicted ice thickness variations disparity between our study projections based on the S1 and LOW2+S2 initial states (Fig. 8). The pronounced discrepancies in the WAIS primarily stem from its vulnerability to oceanic forcing and complex bed topography, projecting an average ice thickness decrease of 50 m by 2100 in S1-based results relative to LOW2+S2-based (Fig. 8). While this study S2 experiment used parameterized melt rates, our in model spin-up, S1 incorporation of observational values reveals enhanced basal melting in the critical WAIS regions like TB (Fig. 2), accelerating dynamic ice loss through processes such as MISI. In contrast, the EAIS regions (WL and GVL) exhibit minor variations, contributing little to sea level rise during projection periods (2050 and 2100; Fig. 8). This regional contrast highlights the WAIS's dominant role in creating divergence from earlier projections, demonstrating its heightened vulnerability to ocean-induced melt rates at the initialization.

## 410 **5 Model Uncertainties**

We maintained consistent model configurations and climate forcings with LOW21 but constrained sub-ice shelf melt rates using observational data during spin up, replacing their TF linear parameterization. The elevated sub-ice shelf melt rates in our simulation experiment S1 (Fig. 2), notably in the Thwaites and Pine Island shelves, modify the initial AIS state. Through an iterative spin-up process, the model iteratively adjusts key variables such as basal ice temperature field, basal friction coefficients, and grounding-line positions to minimize discrepancies between simulation and observation. While the ice-sheet geometries for LOW2+S2 and our study S1 are initialized with identical spin-up, distinct sub-ice shelf melt rates produce divergent ice thermodynamic states, causing the ice sheet to follow unique evolutionary trajectories in projection under identical external forcing, thus altering the potential contributions of sea level rise.

420 The rationale for using the Rignot et al. (2013) basal melt rates in S1 was that the corresponding ocean thermal forcing aligns with the 1975–2012 mean state of the Southern Ocean captured in Schmidtko et al. (2014) dataset (used in S2). However, as these data reflect conditions from approximately a decade ago, they inherently represent a temporal average and do not capture interannual variability in ocean forcing (Adusumilli et al., 2020). Furthermore, Paolo et al. (2023) also observed a widespread slowdown in ice-shelf thinning across the Amundsen, Bellingshausen, and Wilkes sectors, attributing it to changes in ocean forcing and internal ice-dynamic feedbacks. Therefore, S1 simulated results should be interpreted as a response to a steady-state, general ice-shelf basal melting field. Future work should incorporate time-evolving melt rates to better constrain the sensitivity of the AIS to oceanic variability on interannual to decadal timescales.

430 Compared to other prior studies, our sea-level projections from the S1 differ due to variations in ice-sheet model configurations, including model resolution, ice dynamics (particularly stress balance schemes), represented physical processes (calving, hydrology, or bedrock uplift), and initialization methods (data assimilation or spin-up) (Seroussi et al., 2019; Levermann et al., 2020; Klose et al., 2024). Of these factors, the parameterizations of ice melt dynamics

435 ~~contribute most significantly to the uncertainty in sea-level estimates, surpassing those from climate forcing, initialization methods, or the selected physical processes. Given this dominance, ice-model-related uncertainties prevail throughout the entire simulation period (Seroussi et al., 2019, 2023). Therefore, continual model improvement and further exploration of the broader parameter space covered by initial state ensembles are essential to reduce uncertainties in future projections of dynamic mass loss from the AIS (Favier et al., 2019; Coulon et al., 2024; Klose et al., 2024).~~

440 ~~Notably, the present-day AIS may not have been in a steady-state during the observational period, and thus, some of the misfits could be attributed to uncertainties in the observational data used for validation (Martin et al., 2011). While this inference is primarily based on model–observation discrepancies, it may also be influenced by uncertainties inherent in the validation datasets. For example, the BedMachine v3 dataset relies on approximate calculations in regions such as ice-free land, ocean bathymetry, and cavities under ice shelves, potentially introducing spatial biases in thickness estimates (Morlighem et al., 2019). Similarly, the MEASUREs velocity inevitably contains errors in flow direction derived from phase data and speckle tracking during SAR data processing (Mouginot et al., 2019). The apparent model–data mismatch reflects both a non-steady-state of AIS and the challenge of validating model simulations against uncertain modern records, which underscores the need for more accurate and extensive observations to better constrain ice-sheet models and improve the reliability of sea-level projections (Seroussi et al., 2020, 2023).~~ Moreover, global climate models exhibit significant differences in projected global temperature increases, 445 which in turn affect ice dynamics (Golledge et al., 2015; Schlegel et al., 2018; Klose et al., 2024). High-sensitivity climate models within the CMIP6 ensemble, such as IPSL-CM6A-LR (4.6°C), UKESM1-0-LL (5.3°C), and CESM2-WACCM (4.8°C), predict substantial warming over Antarctica, potentially driving extensive melting of the WAIS. 450

## 6 Conclusions

455 ~~By initializing the~~The ice-sheet model ~~with~~ was initialized using two different basal melting schemes: experiment S1 ~~used~~ observed sub-ice shelf melt rates ~~instead of, while S2 employed~~ the TF-linear parameterization ~~employed in a previous~~ to replicate the LOW21 study ~~(LOW21)~~. Following spin-up, the modeled ice geometry ~~aligns closely~~ is consistent with ~~both~~ observations ~~and LOW21 after spin-up in two experiments~~. However, ~~our~~S1 simulated results reveal notable regional variations in ice-sheet dynamics across three marine ice-sheet regions compared to ~~the parameterized method~~S2: the Thwaites Basin in ~~the~~ West Antarctica, Wilkes Land, and George V Land–Terre Adelie 460 in ~~the~~ East Antarctica. In Thwaites Basin, elevated sub-ice shelf melt rates progressively trigger MISI, driving grounding-line retreat that significantly weakens the ice-shelf buttressing effect for upstream glaciers. ~~Our~~Experiment S1 simulations demonstrates 3 m ice thickness discrepancies and 74 m y<sup>-1</sup> ice velocity deviations compared to ~~LOW21's simulations~~S2 results under observational validation. Variations in ocean forcing conditions in Wilkes Land and George V Land–Terre Adelie may alter the thermomechanical features at the grounded ice sheet, 465 which then induce dynamic adjustments, causing approximately 6 m and 44 m y<sup>-1</sup> ~~variations~~differences in ice thickness and surface velocity ~~between S1 and S2~~, respectively.

Despite ~~using~~ identical model configurations and future climate scenarios, ~~our~~ projections ~~from the S1 initial state~~ estimate a 57% higher ~~sea-level~~ contribution ~~of sea level rise~~ (~0.18 m SLE) by 2100 compared to the ~~previous study~~

(LOW21), ~~due to an ensemble results, which includes the projection based on S2. This divergence stems from the~~  
470 different treatment in prescribing sub-ice shelf melt rates during the PISM spin-up. The majority contributor to this  
SLE discrepancy stems from the Amundsen Sea sector in the West Antarctica, a region typical of MISI, which also  
aligns with comparisons to other previous model projection results. In future modeling efforts, we suggest further  
efforts in investigating the sensitivity of ~~Antarctica~~ the Antarctic ice sheet model initializations to critical  
environmental factors before conducting fully prognostic ~~Antarctica ice sheet~~ Antarctica ice sheet AIS simulations, to better constrain the  
475 projected ranges of global sea level rise.

### Code and Data Availability

The Parallel Ice Sheet Model is freely available as open-source code from the PISM GitHub repository  
(<https://github.com/pism/pism>). Bedrock topography and ice thickness data are from the MEaSUREs BedMachine  
Antarctica, Version 3 compilation, available at <https://nsidc.org/data/nsidc-0756/versions/3>. Air temperature,  
480 precipitation, and geothermal heat flux inputs were taken from the ALBMAP version 1 compilation and can be  
downloaded from <http://doi.pangaea.de/10.1594/PANGAEA.734145>. Ice surface velocity used in validation may be  
obtained from MEaSUREs Phase-Based Antarctica Ice Velocity Map, Version 1, available at  
<https://nsidc.org/data/nsidc-0754/versions/1>. The forcing data under RCP and SSP scenarios were sourced from the  
dataset published by Nowicki et al. (2021). The data preprocessing tool used is the publicly available scripts pism-ais  
485 (<https://github.com/pism/pism-ais>).

### Author contribution

Fan GaoFG and Tong ZhangTZ conceived and designed this experiment. Fan GaoFG performed data curation. Qiang  
Shen, Hansheng WangQS, HW, and Tong ZhangTZ acquired funding. ~~HW~~ Hansheng Wang provided resources. Fan  
GaoFG and Tong ZhangTZ conducted the experiments. Fan GaoFG performed simulations. Qiang ShenQS, Liming  
490 JiangLJ, and Yan LiuYL performed validation. ~~C.K. Shum, Yan An~~ CKS, YA, and Xu ZhangXZ conducted the  
visualization. Fan GaoFG wrote the original manuscript draft, and all authors contributed to reviewing and editing the  
manuscript.

### Competing interests

There are no real or perceived conflicts of interest for any author.

### 495 Acknowledgments

We express our heartfelt gratitude to Prof. Lowry for his invaluable mentorship and significant contributions to this  
study. His provision of critical simulation datasets and expert guidance throughout the research process has been  
indispensable. We also sincerely thank Prof. Rignot for generously sharing observational data on Antarctic sub-ice  
shelf melt rates, which greatly enriched our work. Additionally, we extend our sincere appreciation to the Parallel Ice  
500 Sheet Model team for their continuous support and for developing and maintaining the PISM, which was essential to

the success of this research. [We also thank the Editor and three reviewers—including co-reviewers Muruganandham Shivaprakash and Alexander Robel, and an anonymous referee—for their constructive feedback that significantly enhanced this manuscript.](#)

### Financial support

505 This work is supported by the National Natural Science Foundation of China (42374042, 42271133, and 42374045) and the Natural Science Foundation of Wuhan (2024040701010065).

### References

- Adams, C. J. C., Iverson, N. R., Helanow, C., Zoet, L. K., & Bate, C. E. (2021). Softening of Temperate Ice by Interstitial Water. *Frontiers in Earth Science*, 9. <https://doi.org/10.3389/feart.2021.702761>
- 510 [Adusumilli, S., Fricker, H. A., Medley, B., Padman, L., & Siegfried, M. R. \(2020\). Interannual variations in meltwater input to the Southern Ocean from Antarctic ice shelves. \*Nature Geoscience\*, 13\(9\), 616-620. <https://doi.org/10.1038/s41561-020-0616-z>](#)
- Aitken, A. R. A., Young, D. A., Ferraccioli, F., Betts, P. G., Greenbaum, J. S., Richter, T. G., Roberts, J. L., Blankenship, D. D., & Siegert, M. J. (2014). The subglacial geology of Wilkes Land, East Antarctica. *Geophysical Research Letters*, 41(7), 2390-2400. <https://doi.org/10.1002/2014gl059405>
- 515 Albrecht, T., Martin, M., Haseloff, M., Winkelmann, R., & Levermann, A. (2011). Parameterization for subgrid-scale motion of ice-shelf calving fronts. *The Cryosphere*, 5(1), 35-44. <https://doi.org/10.5194/tc-5-35-2011>
- Albrecht, T., Winkelmann, R., & Levermann, A. (2020). Glacial-cycle simulations of the Antarctic Ice Sheet with the Parallel Ice Sheet Model (PISM) – Part 2: Parameter ensemble analysis. *The Cryosphere*, 14(2), 633-656. <https://doi.org/10.5194/tc-14-633-2020>
- 520 Alevropoulos-Borrill, A. V., Nias, I. J., Payne, A. J., Gollidge, N. R., & Bingham, R. J. (2020). Ocean-forced evolution of the Amundsen Sea catchment, West Antarctica, by 2100. *The Cryosphere*, 14(4), 1245-1258. <https://doi.org/10.5194/tc-14-1245-2020>
- Beckmann, A. and Goosse, H. (2003). A parametrization of ice shelf-ocean interaction for climate models, *Ocean Model.*, 5(2), 157–170. [https://doi.org/10.1016/S1463-5003\(02\)00019-7](https://doi.org/10.1016/S1463-5003(02)00019-7)
- 525 Barthel, A., Agosta, C., Little, C. M., Hattermann, T., Jourdain, N. C., Goelzer, H., Nowicki, S., Seroussi, H., Straneo, F., & Bracegirdle, T. J. (2020). CMIP5 model selection for ISMIP6 ice sheet model forcing: Greenland and Antarctica. *The Cryosphere*, 14(3), 855-879. <https://doi.org/10.5194/tc-14-855-2020>
- Berdahl, M., Leguy, G., Lipscomb, W. H., Urban, N. M., & Hoffman, M. J. (2023). Exploring ice sheet model sensitivity to ocean thermal forcing and basal sliding using the Community Ice Sheet Model (CISM). *The Cryosphere*, 17(4), 1513-1543. <https://doi.org/10.5194/tc-17-1513-2023>
- 530 Bindschadler, R. A., Nowicki, S., Abe-Ouchi, A., Aschwanden, A., Choi, H., Fastook, J., Granzow, G., Greve, R., Gutowski, G., Herzfeld, U., Jackson, C., Johnson, J., Khroulev, C., Levermann, A., Lipscomb, W. H., Martin, M. A., Morlighem, M., Parizek, B. R., Pollard, D., Price, S. F., Ren, D., Saito, F., Sato, T., Seddik, H., Seroussi, H., Takahashi, K., Walker, R., & Wang, W. L. (2013). Ice-sheet model sensitivities to environmental forcing and their use in projecting future sea level (the SeaRISE project). *Journal of Glaciology*, 59(214), 195-224. <https://doi.org/10.3189/2013JoG12J125>
- 535 Boening, C., Lebsock, M., Landerer, F., & Stephens, G. (2012). Snowfall-driven mass change on the East Antarctic ice sheet. *Geophysical Research Letters*, 39(21). <https://doi.org/10.1029/2012gl053316>
- 540 Bueler, E., & Brown, J. (2009). Shallow shelf approximation as a “sliding law” in a thermomechanically coupled ice sheet model. *Journal of Geophysical Research*, 114(F3). <https://doi.org/10.1029/2008jf001179>
- Bueler, E., Brown, J., & Lingle, C. (2007). Exact solutions to the thermomechanically coupled shallow-ice approximation: effective tools for verification. *Journal of Glaciology*, 53(182), 499-516. <https://doi.org/10.3189/002214307783258396>
- 545 Calov, R., & Greve, R. (2017). A semi-analytical solution for the positive degree-day model with stochastic temperature variations. *Journal of Glaciology*, 51(172), 173-175. <https://doi.org/10.3189/172756505781829601>

- Chambers, C., Greve, R., Obase, T., Saito, F., & Abe-Ouchi, A. (2021). Mass loss of the Antarctic ice sheet until the year 3000 under a sustained late-21st-century climate. *Journal of Glaciology*, 1-13. <https://doi.org/10.1017/jog.2021.124>
- 550 Church, J., Clark, P., Cazenave, A., Gregory, J., Jevrejeva, S., Levermann, A., Merrifield, M., Milne, G., Nerem, R., & Nunn, P. (2013). "Chapter 13: Sea Level Change" in *Climate Change 2013: The Physical Science Basis: Contribution of Working Group I to the Fifth Assessment Report of the Intergovernmental Panel on Climate Change*.
- 555 Clarke, G. K. C. (2005). Subglacial Processes. *Annual Review of Earth and Planetary Sciences*, 33(1), 247-276. <https://doi.org/10.1146/annurev.earth.33.092203.122621>
- Cornford, S. L., Martin, D. F., Payne, A. J., Ng, E. G., Le Brocq, A. M., Gladstone, R. M., Edwards, T. L., Shannon, S. R., Agosta, C., van den Broeke, M. R., Hellmer, H. H., Krinner, G., Ligtenberg, S. R. M., Timmermann, R., & Vaughan, D. G. (2015). Century-scale simulations of the response of the West Antarctic Ice Sheet to a warming climate. *The Cryosphere*, 9(4), 1579-1600. <https://doi.org/10.5194/tc-9-1579-2015>
- 560 Cornford, S. L., Seroussi, H., Asay-Davis, X. S., Gudmundsson, G. H., Arthern, R., Borstad, C., Christmann, J., Dias dos Santos, T., Feldmann, J., Goldberg, D., Hoffman, M. J., Humbert, A., Kleiner, T., Leguy, G., Lipscomb, W. H., Merino, N., Durand, G., Morlighem, M., Pollard, D., Rückamp, M., Williams, C. R., & Yu, H. (2020). Results of the third Marine Ice Sheet Model Intercomparison Project (MISMIP+). *The Cryosphere*, 14(7), 2283-2301. <https://doi.org/10.5194/tc-14-2283-2020>
- 565 Coulon, V., Klose, A. K., Kittel, C., Edwards, T., Turner, F., Winkelmann, R., & Pattyn, F. (2024). Disentangling the drivers of future Antarctic ice loss with a historically calibrated ice-sheet model. *The Cryosphere*, 18(2), 653-681. <https://doi.org/10.5194/tc-18-653-2024>
- Cuffey, K. M., & Paterson, W. S. B. (2010). *The physics of glaciers*. Academic Press.
- 570 Dawson, E. J., Schroeder, D. M., Chu, W., Mantelli, E., & Seroussi, H. (2022). Ice mass loss sensitivity to the Antarctic ice sheet basal thermal state. *Nature Communications*, 13(1). <https://doi.org/10.1038/s41467-022-32632-2>
- DeConto, R. M., & Pollard, D. (2016). Contribution of Antarctica to past and future sea-level rise. *Nature*, 531(7596), 591-597. <https://doi.org/10.1038/nature17145>
- Depoorter, M. A., Bamber, J. L., Griggs, J. A., Lenaerts, J. T. M., Ligtenberg, S. R. M., van den Broeke, M. R., & Moholdt, G. (2013). Calving fluxes and basal melt rates of Antarctic ice shelves. *Nature*, 502(7469), 89-92. <https://doi.org/10.1038/nature12567>
- 575 Dinniman, M., Asay-Davis, X., Galton-Fenzi, B., Holland, P., Jenkins, A., & Timmermann, R. (2016). Modeling Ice Shelf/Ocean Interaction in Antarctica: A Review. *Oceanography*, 29(4), 144-153. <https://doi.org/10.5670/oceanog.2016.106>
- 580 Edwards, T. L., Brandon, M. A., Durand, G., Edwards, N. R., Gолledge, N. R., Holden, P. B., Nias, I. J., Payne, A. J., Ritz, C., & Wernecke, A. (2019). Revisiting Antarctic ice loss due to marine ice-cliff instability. *Nature*, 566(7742), 58-64. <https://doi.org/10.1038/s41586-019-0901-4>
- Edwards, T. L., Nowicki, S., Marzeion, B., Hock, R., Goelzer, H., Seroussi, H., Jourdain, N. C., Slater, D. A., Turner, F. E., Smith, C. J., McKenna, C. M., Simon, E., Abe-Ouchi, A., Gregory, J. M., Larour, E., Lipscomb, W. H., Payne, A. J., Shepherd, A., Agosta, C., Alexander, P., Albrecht, T., Anderson, B., Asay-Davis, X., Aschwanden, A., Barthel, A., Bliss, A., Calov, R., Chambers, C., Champollion, N., Choi, Y., Cullather, R., Cuzzone, J., Dumas, C., Felikson, D., Fettweis, X., Fujita, K., Galton-Fenzi, B. K., Gladstone, R., Gолledge, N. R., Greve, R., Hattermann, T., Hoffman, M. J., Humbert, A., Huss, M., Huybrechts, P., Immerzeel, W., Kleiner, T., Kraaijenbrink, P., Le Clec'h, S., Lee, V., Leguy, G. R., Little, C. M., Lowry, D. P., Mallet, J. H., Martin, D. F., Maussion, F., Morlighem, M., O'Neill, J. F., Nias, I., Pattyn, F., Pelle, T., Price, S. F., Quiquet, A., Radic, V., Reese, R., Rounce, D. R., Rückamp, M., Sakai, A., Shafer, C., Schlegel, N. J., Shannon, S., Smith, R. S., Straneo, F., Sun, S., Tarasov, L., Trusel, L. D., Van Breedam, J., van de Wal, R., van den Broeke, M., Winkelmann, R., Zekollari, H., Zhao, C., Zhang, T., & Zwinger, T. (2021). Projected land ice contributions to twenty-first-century sea level rise. *Nature*, 593(7857), 74-82. <https://doi.org/10.1038/s41586-021-03302-y>
- 595 [Favier, L., Jourdain, N. C., Jenkins, A., Merino, N., Durand, G., Gagliardini, O., Gillet-Chaulet, F., & Mathiot, P. \(2019\). Assessment of sub-shelf melting parameterisations using the ocean - ice-sheet coupled model NEMO\(v3.6\) - Elmer/Ice\(v8.3\). \*Geoscientific Model Development\*, 12\(6\), 2255-2283. <https://doi.org/10.5194/gmd-12-2255-2019>](https://doi.org/10.5194/gmd-12-2255-2019)
- 600 [Feldmann, J., Albrecht, T., Khroulev, C., Pattyn, F., & Levermann, A. \(2017\). Resolution-dependent performance of grounding line motion in a shallow model compared with a full-Stokes model according to the MISMIP3d intercomparison. \*Journal of Glaciology\*, 60\(220\), 353-360. <https://doi.org/10.3189/2014JG13J093>](https://doi.org/10.3189/2014JG13J093)

- Feldmann, J., & Levermann, A. (2023). Timescales of outlet-glacier flow with negligible basal friction: theory, observations, and modeling. *The Cryosphere*, 17(1), 327-348. <https://doi.org/10.5194/tc-17-327-2023>
- 605 Feldmann, J., Levermann, A., & Winkelmann, R. (2024). Hysteresis of idealized, instability-prone outlet glaciers in response to pinning-point buttressing variation. *The Cryosphere*, 18(9), 4011-4028. <https://doi.org/10.5194/tc-18-4011-2024>
- Fowler, A., Murray, T., & Ng, F. (2001). Thermally controlled glacier surging. *Journal of Glaciology*, 47(159), 527-538. <https://doi.org/10.3189/172756501781831792>
- 610 Frederick, B. C., Young, D. A., Blankenship, D. D., Richter, T. G., Kempf, S. D., Ferraccioli, F., & Siegert, M. J. (2016). Distribution of subglacial sediments across the Wilkes Subglacial Basin, East Antarctica. *Journal of Geophysical Research: Earth Surface*, 121(4), 790-813. <https://doi.org/10.1002/2015jf003760>
- [Gagliardini, O., Durand, G., Zwinger, T., Hindmarsh, R. C. A., & Le Meur, E. \(2010\). Coupling of ice - shelf melting and buttressing is a key process in ice - sheets dynamics. \*Geophysical Research Letters\*, 37\(14\). <https://doi.org/10.1029/2010gl043334>](https://doi.org/10.1029/2010gl043334)
- 615 Garbe, J., Albrecht, T., Levermann, A., Donges, J. F., & Winkelmann, R. (2020). The hysteresis of the Antarctic Ice Sheet. *Nature*, 585(7826), 538-544. <https://doi.org/10.1038/s41586-020-2727-5>
- Goldberg, D., Holland, D. M., & Schoof, C. (2009). Grounding line movement and ice shelf buttressing in marine ice sheets. *Journal of Geophysical Research: Earth Surface*, 114(F4). <https://doi.org/10.1029/2008jf001227>
- 620 Golledge, N. R., Kowalewski, D. E., Naish, T. R., Levy, R. H., Fogwill, C. J., & Gasson, E. G. (2015). The multi-millennial Antarctic commitment to future sea-level rise. *Nature*, 526(7573), 421-425. <https://doi.org/10.1038/nature15706>
- Goodwin, B. P., Mosley-Thompson, E., Wilson, A. B., Porter, S. E., & Sierra-Hernandez, M. R. (2016). Accumulation Variability in the Antarctic Peninsula: The Role of Large-Scale Atmospheric Oscillations and Their Interactions. *Journal of Climate*, 29(7), 2579-2596. <https://doi.org/10.1175/JCLI-D-15-0354.1>
- 625 Greenbaum, J., Blankenship, D., Young, D., Richter, T., Roberts, J., Aitken, A., Legresy, B., Schroeder, D., Warner, R., & Van Ommen, T. (2015). Ocean access to a cavity beneath Totten Glacier in East Antarctica. *Nature Geoscience*, 8(4), 294-298. <https://doi.org/10.1038/ngeo2388>
- Gudmundsson, G. H. (2003). Transmission of basal variability to a glacier surface. *Journal of Geophysical Research: Solid Earth*, 108(B5). <https://doi.org/10.1029/2002jb002107>
- 630 Gudmundsson, G. H. (2013). Ice-shelf buttressing and the stability of marine ice sheets. *The Cryosphere*, 7(2), 647-655. <https://doi.org/10.5194/tc-7-647-2013>
- Hellmer, H. H. and Olbers, D. J. (1989). A Two-Dimensional Model for the Thermohaline Circulation Under an Ice Shelf, *Antarctic Science*, 1(04), 325-336. <https://doi.org/10.1017/S0954102089000490>
- 635 [Hill, E. A., Gudmundsson, G. H., & Chandler, D. M. \(2024\). Ocean warming as a trigger for irreversible retreat of the Antarctic ice sheet. \*Nature Climate Change\*, 14\(11\), 1165-1171. <https://doi.org/10.1038/s41558-024-02134-8>](https://doi.org/10.1038/s41558-024-02134-8)
- Hindmarsh, R. C. (2006). The role of membrane-like stresses in determining the stability and sensitivity of the Antarctic ice sheets: back pressure and grounding line motion. *Philos Trans A Math Phys Eng Sci*, 364(1844), 1733-1767. <https://doi.org/10.1098/rsta.2006.1797>
- 640 [Hock, R., Bliss, A., Marzeion, B. E. N., Giesen, R. H., Hirabayashi, Y., Huss, M., Radić, V., & Slangen, A. B. A. \(2019\). GlacierMIP - A model intercomparison of global-scale glacier mass-balance models and projections. \*Journal of Glaciology\*, 65\(251\), 453-467. <https://doi.org/10.1017/jog.2019.22>](https://doi.org/10.1017/jog.2019.22)
- Holland, D. M. and Jenkins, A. (1999). Modeling Thermodynamic Ice Ocean Interactions at the Base of an Ice Shelf, *Journal of Physical Oceanography*, 29, 1787-1800. [https://doi.org/10.1175/1520-0485\(1999\)029<1787:MTIOIA>2.0.CO;2](https://doi.org/10.1175/1520-0485(1999)029<1787:MTIOIA>2.0.CO;2)
- 645 Holland, P. R., Bracegirdle, T. J., Dutrieux, P., Jenkins, A., & Steig, E. J. (2019). West Antarctic ice loss influenced by internal climate variability and anthropogenic forcing. *Nature Geoscience*, 12(9), 718-724. <https://doi.org/10.1038/s41561-019-0420-9>
- 650 [Huybers, K., Roe, G., & Conway, H. \(2017\). Basal topographic controls on the stability of the West Antarctic ice sheet: lessons from Foundation Ice Stream. \*Annals of Glaciology\*, 58\(75pt2\), 193-198. <https://doi.org/10.1017/aog.2017.9>](https://doi.org/10.1017/aog.2017.9)
- Jacobs, S. S., Jenkins, A., Giulivi, C. F., & Dutrieux, P. (2011). Stronger ocean circulation and increased melting under Pine Island Glacier ice shelf. *Nature Geoscience*, 4(8), 519-523. <https://doi.org/10.1038/ngeo1188>
- 655 Joughin, I., E. Smith, B., & Brooke, M. (2014). Marine Ice Sheet Collapse Potentially Under Way for the Thwaites Glacier Basin, West Antarctica. *Science*, 344(6185), 735-738. <https://doi.org/10.1126/science.124905>

- Jourdain, N. C., Asay-Davis, X., & Hattermann, T. (2020). A protocol for calculating basal melt rates in the ISMIP6 Antarctic ice sheet projections. *The Cryosphere*, *14*, 3111-3134. <https://doi.org/10.5194/tc-14-3111-2020>
- 660 Kamworapan, S., Bich Thao, P. T., Gheewala, S. H., Pimonsree, S., & Prueksakorn, K. (2021). Evaluation of CMIP6 GCMs for simulations of temperature over Thailand and nearby areas in the early 21st century. *Heliyon*, *7*(11), e08263. <https://doi.org/10.1016/j.heliyon.2021.e08263>
- Klose, A. K., Coulon, V., Pattyn, F., & Winkelmann, R. (2024). The long-term sea-level commitment from Antarctica. *The Cryosphere*, *18*(9), 4463-4492. <https://doi.org/10.5194/tc-18-4463-2024>
- 665 Konrad, H., Shepherd, A., Gilbert, L., Hogg, A. E., McMillan, M., Muir, A., & Slater, T. (2018). Net retreat of Antarctic glacier grounding lines. *Nature Geoscience*, *11*(4), 258-262. <https://doi.org/10.1038/s41561-018-0082-z>
- Lazeroms, W. M. J., Jenkins, A., Gudmundsson, G. H., & van de Wal, R. S. W. (2018). Modeling present-day basal melt rates for Antarctic ice shelves using a parametrization of buoyant meltwater plumes. *The Cryosphere*, *12*(1), 49-70. <https://doi.org/10.5194/tc-12-49-2018>
- 670 [Leguy, G. R., Asay-Davis, X. S., & Lipscomb, W. H. \(2014\). Parameterization of basal friction near grounding lines in a one-dimensional ice sheet model. \*The Cryosphere\*, \*8\*\(4\), 1239-1259. <https://doi.org/10.5194/tc-8-1239-2014>](#)
- Levermann, A., Winkelmann, R., Albrecht, T., Goelzer, H., Golledge, N. R., Greve, R., Huybrechts, P., Jordan, J., Leguy, G., Martin, D., Morlighem, M., Pattyn, F., Pollard, D., Quiquet, A., Rodehacke, C., Seroussi, H., Sutter, J., Zhang, T., Van Breedam, J., Calov, R., DeConto, R., Dumas, C., Garbe, J., Gudmundsson, G. H., Hoffman, M. J., Humbert, A., Kleiner, T., Lipscomb, W. H., Meinshausen, M., Ng, E., Nowicki, S. M. J., Perego, M., Price, S. F., Saito, F., Schlegel, N.-J., Sun, S., & van de Wal, R. S. W. (2020). Projecting Antarctica's contribution to future sea level rise from basal ice shelf melt using linear response functions of 16 ice sheet models (LARMIP-2). *Earth System Dynamics*, *11*(1), 35-76. <https://doi.org/10.5194/esd-11-35-2020>
- 675 Li, L., Aitken, A. R., Lindsay, M. D., & Kulesa, B. (2022). Sedimentary basins reduce stability of Antarctic ice streams through groundwater feedbacks. *Nature Geoscience*, *15*(8), 645-650. <https://doi.org/10.1038/s41561-022-00992-5>
- 680 Li, Q., England, M. H., Hogg, A. M., Rintoul, S. R., & Morrison, A. K. (2023). Abyssal ocean overturning slowdown and warming driven by Antarctic meltwater. *Nature*, *615*(7954), 841-847. <https://doi.org/10.1038/s41586-023-05762-w>
- 685 Lipscomb, W. H., Price, S. F., Hoffman, M. J., Leguy, G. R., Bennett, A. R., Bradley, S. L., Evans, K. J., Fyke, J. G., Kennedy, J. H., Perego, M., Ranken, D. M., Sacks, W. J., Salinger, A. G., Vargo, L. J., & Worley, P. H. (2019). Description and evaluation of the Community Ice Sheet Model (CISM) v2.1. *Geoscientific Model Development*, *12*(1), 387-424. <https://doi.org/10.5194/gmd-12-387-2019>
- 690 Li, X., Rignot, E., Mouginot, J., & Scheuchl, B. (2016). Ice flow dynamics and mass loss of Totten Glacier, East Antarctica, from 1989 to 2015. *Geophysical Research Letters*, *43*(12), 6366-6373. <https://doi.org/10.1002/2016gl069173>
- 695 Lowry, D. P., Krapp, M., Golledge, N. R., & Alevropoulos-Borrill, A. (2021). The influence of emissions scenarios on future Antarctic ice loss is unlikely to emerge this century. *Communications Earth & Environment*, *2*(1). <https://doi.org/10.1038/s43247-021-00289-2>
- Martin, M. A., Winkelmann, R., Haseloff, M., Albrecht, T., Bueler, E., Khroulev, C., & Levermann, A. (2011). The Potsdam Parallel Ice Sheet Model (PISM-PIK) – Part 2: Dynamic equilibrium simulation of the Antarctic ice sheet. *The Cryosphere*, *5*(3), 727-740. <https://doi.org/10.5194/tc-5-727-2011>
- 700 Mengel, M., & Levermann, A. (2014). Ice plug prevents irreversible discharge from East Antarctica. *Nature Climate Change*, *4*(6), 451-455. <https://doi.org/10.1038/nclimate2226>
- Miles, B. W. J., & Bingham, R. G. (2024). Progressive unanchoring of Antarctic ice shelves since 1973. *Nature*, *626*(8000), 785-791. <https://doi.org/10.1038/s41586-024-07049-0>
- 705 Miles, B. W. J., Stokes, C. R., Jamieson, S. S. R., Jordan, J. R., Gudmundsson, G. H., & Jenkins, A. (2022). High spatial and temporal variability in Antarctic ice discharge linked to ice shelf buttressing and bed geometry. *Scientific Reports*, *12*(1), 10968. <https://doi.org/10.1038/s41598-022-13517-2>
- 710 Morlighem, M., Rignot, E., Binder, T., Blankenship, D., Drews, R., Eagles, G., Eisen, O., Ferraccioli, F., Forsberg, R., Fretwell, P., Goel, V., Greenbaum, J. S., Gudmundsson, H., Guo, J., Helm, V., Hofstede, C., Howat, I., Humbert, A., Jokat, W., Karlsson, N. B., Lee, W. S., Matsuoka, K., Millan, R., Mouginot, J., Paden, J., Pattyn, F., Roberts, J., Rosier, S., Ruppel, A., Seroussi, H., Smith, E. C., Steinhage, D., Sun, B., Broeke, M. R. v. d., Ommen, T. D. v., Wesse, M. v., & Young, D. A. (2019). Deep glacial troughs and stabilizing ridges

- unveiled beneath the margins of the Antarctic ice sheet. *Nature Geoscience*, 13(2), 132-137. <https://doi.org/10.1038/s41561-019-0510-8>
- 715 Mouginit, J., Rignot, E., & Scheuchl, B. (2019). Continent-Wide, Interferometric SAR Phase, Mapping of Antarctic Ice Velocity. *Geophysical Research Letters*, 46(16), 9710-9718. <https://doi.org/https://doi.org/10.1029/2019GL083826>
- 720 Noble, T. L., Rohling, E. J., Aitken, A. R. A., Bostock, H. C., Chase, Z., Gomez, N., Jong, L. M., King, M. A., Mackintosh, A. N., McCormack, F. S., McKay, R. M., Menviel, L., Phipps, S. J., Weber, M. E., Fogwill, C. J., Gayen, B., Gollidge, N. R., Gwyther, D. E., Hogg, A. M., Martos, Y. M., Pena-Molino, B., Roberts, J., Fliedert, T., & Williams, T. (2020). The Sensitivity of the Antarctic Ice Sheet to a Changing Climate: Past, Present, and Future. *Reviews of Geophysics*, 58(4). <https://doi.org/10.1029/2019rg000663>
- Nowicki, S. M. J., Payne, T., Larour, E., Seroussi, H., Goelzer, H., Lipscomb, W., Gregory, J., Abe-Ouchi, A., & Shepherd, A. (2016). Ice Sheet Model Intercomparison Project (ISMIP6) contribution to CMIP6. *Geoscientific Model Development*, 9(12), 4521-4545. <https://doi.org/10.5194/gmd-9-4521-2016>
- 725 [Nowicki, S., Goelzer, H., Seroussi, H., Payne, A. J., Lipscomb, W. H., Abe-Ouchi, A., Agosta, C., Alexander, P., Asay-Davis, X. S., Barthel, A., Bracegirdle, T. J., Cullather, R., Felikson, D., Fettweis, X., Gregory, J. M., Hattermann, T., Jourdain, N. C., Kuipers Munneke, P., Larour, E., Little, C. M., Morlighem, M., Nias, I., Shepherd, A., Simon, E., Slater, D., Smith, R. S., Straneo, F., Trusel, L. D., van den Broeke, M. R., & van de Wal, R. \(2020\). Experimental protocol for sea level projections from ISMIP6 stand-alone ice sheet models. \*The Cryosphere\*, 14\(7\), 2331-2368. <https://doi.org/10.5194/tc-14-2331-2020>](https://doi.org/10.5194/gmd-9-4521-2016)
- 730 [Nowicki, S., Simon, E., & ISMIP6 Team. \(2021\). ISMIP6 21st Century Forcing Datasets \[Data set\]. The Ghub. <https://doi.org/10.5281/zenodo.11176009>](https://doi.org/10.5281/zenodo.11176009)
- Ohmura, A. (2001). Physical basis for the temperature-based melt-index method. *Journal of applied Meteorology*, 40(4), 753-761. [https://doi.org/10.1175/1520-0450\(2001\)040%3C0753:PBFTTB%3E2.0.CO;2](https://doi.org/10.1175/1520-0450(2001)040%3C0753:PBFTTB%3E2.0.CO;2)
- 735 Pattyn, F., Schoof, C., Perichon, L., Hindmarsh, R. C. A., Bueller, E., de Fleurian, B., Durand, G., Gagliardini, O., Gladstone, R., Goldberg, D., Gudmundsson, G. H., Huybrechts, P., Lee, V., Nick, F. M., Payne, A. J., Pollard, D., Rybak, O., Saito, F., & Vieli, A. (2012). Results of the Marine Ice Sheet Model Intercomparison Project, MISMIP. *The Cryosphere*, 6(3), 573-588. <https://doi.org/10.5194/tc-6-573-2012>
- Paolo, F. S., Fricker, H. A., & Padman, L. (2015). Volume loss from Antarctic ice shelves is accelerating. *Science*, 348(6232), 327-331. <https://doi.org/10.1126/science.aaa0940>
- 740 [Paolo, F. S., Gardner, A. S., Greene, C. A., Nilsson, J., Schodlok, M. P., Schlegel, N.-J., & Fricker, H. A. \(2023\). Widespread slowdown in thinning rates of West Antarctic ice shelves. \*The Cryosphere\*, 17\(8\), 3409-3433. <https://doi.org/10.5194/tc-17-3409-2023>](https://doi.org/10.5194/tc-17-3409-2023)
- 745 Payne, A. J., Nowicki, S., Abe-Ouchi, A., Agosta, C., Alexander, P., Albrecht, T., Asay-Davis, X., Aschwanden, A., Barthel, A., Bracegirdle, T. J., Calov, R., Chambers, C., Choi, Y., Cullather, R., Cuzzone, J., Dumas, C., Edwards, T. L., Felikson, D., Fettweis, X., Galton-Fenzi, B. K., Goelzer, H., Gladstone, R., Gollidge, N. R., Gregory, J. M., Greve, R., Hattermann, T., Hoffman, M. J., Humbert, A., Huybrechts, P., Jourdain, N. C., Kleiner, T., Munneke, P. K., Larour, E., Le clec'h, S., Lee, V., Leguy, G., Lipscomb, W. H., Little, C. M., Lowry, D. P., Morlighem, M., Nias, I., Pattyn, F., Pelle, T., Price, S. F., Quiquet, A., Reese, R., Rückamp, M., Schlegel, N. J., Seroussi, H., Shepherd, A., Simon, E., Slater, D., Smith, R. S., Straneo, F., Sun, S., Tarasov, L., Trusel, L. D., Van Breedam, J., Wal, R., Broeke, M., Winkelmann, R., Zhao, C., Zhang, T., & Zwinger, T. (2021). Future Sea Level Change Under Coupled Model Intercomparison Project Phase 5 and Phase 6 Scenarios From the Greenland and Antarctic Ice Sheets. *Geophysical Research Letters*, 48(16). <https://doi.org/10.1029/2020gl091741>
- 755 Pelle, T., Morlighem, M., & Bondzio, J. H. (2019). Brief communication: PICOP, a new ocean melt parameterization under ice shelves combining PICO and a plume model. *The Cryosphere*, 13(3), 1043-1049. <https://doi.org/10.5194/tc-13-1043-2019>
- Pittard, M. L., Whitehouse, P. L., Bentley, M. J., & Small, D. (2022). An ensemble of Antarctic deglacial simulations constrained by geological observations. *Quaternary Science Reviews*, 298. <https://doi.org/10.1016/j.quascirev.2022.107800>
- 760 Pollard, D., & DeConto, R. M. (2012). Description of a hybrid ice sheet-shelf model, and application to Antarctica. *Geoscientific Model Development*, 5(5), 1273-1295. <https://doi.org/10.5194/gmd-5-1273-2012>
- Pritchard, H. D., Ligtenberg, S. R. M., Fricker, H. A., Vaughan, D. G., van den Broeke, M. R., & Padman, L. (2012). Antarctic ice-sheet loss driven by basal melting of ice shelves. *Nature*, 484(7395), 502-505. <https://doi.org/10.1038/nature10968>
- 765 Reese, R., Albrecht, T., Mengel, M., Asay-Davis, X., & Winkelmann, R. (2018). Antarctic sub-shelf melt rates via PICO. *The Cryosphere*, 12(6), 1969-1985. <https://doi.org/10.5194/tc-12-1969-2018>

770 Reese, R., Levermann, A., Albrecht, T., Seroussi, H., & Winkelmann, R. (2020). The role of history and strength of the oceanic forcing in sea level projections from Antarctica with the Parallel Ice Sheet Model. *The Cryosphere*, 14(9), 3097-3110. <https://doi.org/10.5194/tc-14-3097-2020>

Rignot, E., Bamber, J. L., van den Broeke, M. R., Davis, C., Li, Y., van de Berg, W. J., & van Meijgaard, E. (2008). Recent Antarctic ice mass loss from radar interferometry and regional climate modeling. *Nature Geoscience*, 1(2), 106-110. <https://doi.org/10.1038/ngeo102>

775 Rignot, E., Jacobs, R., Mouginot, J., & Scheuchl, B. (2013). Ice-Shelf Melting Around Antarctica. *Science*, 341, 266. <https://doi.org/10.1126/science.1235798>

Rignot, E., Mouginot, J., Scheuchl, B., van den Broeke, M., van Wessem, M. J., & Morlighem, M. (2019). Four decades of Antarctic Ice Sheet mass balance from 1979-2017. *Proc Natl Acad Sci USA*, 116(4), 1095-1103. <https://doi.org/10.1073/pnas.1812883116>

780 Ritz, C., Edwards, T. L., Durand, G., Payne, A. J., Peyaud, V., & Hindmarsh, R. C. A. (2015). Potential sea-level rise from Antarctic ice-sheet instability constrained by observations. *Nature*, 528(7580), 115-118. <https://doi.org/10.1038/nature16147>

Rounce, D. R., Regine Hock, Fabien Maussion, Romain Hugonnet, William Kochtitzky, Matthias Huss, Etienne Berthier, Douglas Brinkerhoff, Loris Compagno, Luke Copland, Daniel Farinotti, Brian Menounos, & McNabb, R. W. (2023). Global glacier change in the 21st century: Every increase in temperature matters. *Science*, 379(6627), 78-83. <https://doi.org/10.1126/science.abo1324>

785 Schlegel, N.-J., Seroussi, H., Schodlok, M. P., Larour, E. Y., Boening, C., Limonadi, D., Watkins, M. M., Morlighem, M., & van den Broeke, M. R. (2018). Exploration of Antarctic Ice Sheet 100-year contribution to sea level rise and associated model uncertainties using the ISSM framework. *The Cryosphere*, 12(11), 3511-3534. <https://doi.org/10.5194/tc-12-3511-2018>

790 Schlemm, T., Feldmann, J., Winkelmann, R., & Levermann, A. (2022). Stabilizing effect of mélange buttressing on the marine ice-cliff instability of the West Antarctic Ice Sheet. *The Cryosphere*, 16(5), 1979-1996. <https://doi.org/10.5194/tc-16-1979-2022>

Schmidtko, S., Heywood, K. J., Thompson, A. F., & Aoki, S. (2014). Multidecadal warming of Antarctic waters. *Science*, 346(6214), 1227-1231. <https://doi.org/10.1126/science.1256117>

795 Schoof, C. (2007). Ice sheet grounding line dynamics: Steady states, stability, and hysteresis. *Journal of Geophysical Research: Earth Surface*, 112(F3). <https://doi.org/10.1029/2006jf000664>

Seroussi, H., Morlighem, M., Rignot, E., Mouginot, J., Larour, E., Schodlok, M., & Khazendar, A. (2014). Sensitivity of the dynamics of Pine Island Glacier, West Antarctica, to climate forcing for the next 50 years. *The Cryosphere*, 8(5), 1699-1710. <https://doi.org/10.5194/tc-8-1699-2014>

800 Seroussi, H., Nowicki, S., Payne, A. J., Goelzer, H., Lipscomb, W. H., Abe-Ouchi, A., Agosta, C., Albrecht, T., Asay-Davis, X., Barthel, A., Calov, R., Cullather, R., Dumas, C., Galton-Fenzi, B. K., Gladstone, R., Gолledge, N. R., Gregory, J. M., Greve, R., Hattermann, T., Hoffman, M. J., Humbert, A., Huybrechts, P., Jourdain, N. C., Kleiner, T., Larour, E., Leguy, G. R., Lowry, D. P., Little, C. M., Morlighem, M., Pattyn, F., Pelle, T., Price, S. F., Quiquet, A., Reese, R., Schlegel, N.-J., Shepherd, A., Simon, E., Smith, R. S., Straneo, F., Sun, S., Trusel, L. D., Van Breedam, J., van de Wal, R. S. W., Winkelmann, R., Zhao, C., Zhang, T., & Zwinger, T. (2020). ISMIP6 Antarctica: a multi-model ensemble of the Antarctic ice sheet evolution over the 21st century. *The Cryosphere*, 14(9), 3033-3070. <https://doi.org/10.5194/tc-14-3033-2020>

805 Seroussi, H., Nowicki, S., Simon, E., Abe-Ouchi, A., Albrecht, T., Brondex, J., Cornford, S., Dumas, C., Gillet-Chaulet, F., Goelzer, H., Gолledge, N. R., Gregory, J. M., Greve, R., Hoffman, M. J., Humbert, A., Huybrechts, P., Kleiner, T., Larour, E., Leguy, G., Lipscomb, W. H., Lowry, D., Mengel, M., Morlighem, M., Pattyn, F., Payne, A. J., Pollard, D., Price, S. F., Quiquet, A., Reerink, T. J., Reese, R., Rodehacke, C. B., Schlegel, N.-J., Shepherd, A., Sun, S., Sutter, J., Van Breedam, J., van de Wal, R. S. W., Winkelmann, R., & Zhang, T. (2019). initMIP-Antarctica: an ice sheet model initialization experiment of ISMIP6. *The Cryosphere*, 13(5), 1441-1471. <https://doi.org/10.5194/tc-13-1441-2019>

815 [Seroussi, H., Verjans, V., Nowicki, S., Payne, A. J., Goelzer, H., Lipscomb, W. H., Abe-Ouchi, A., Agosta, C., Albrecht, T., Asay-Davis, X., Barthel, A., Calov, R., Cullather, R., Dumas, C., Galton-Fenzi, B. K., Gladstone, R., Gолledge, N. R., Gregory, J. M., Greve, R., Hattermann, T., Hoffman, M. J., Humbert, A., Huybrechts, P., Jourdain, N. C., Kleiner, T., Larour, E., Leguy, G. R., Lowry, D. P., Little, C. M., Morlighem, M., Pattyn, F., Pelle, T., Price, S. F., Quiquet, A., Reese, R., Schlegel, N.-J., Shepherd, A., Simon, E., Smith, R. S., Straneo, F., Sun, S., Trusel, L. D., Van Breedam, J., Van Katwyk, P., van de Wal, R. S. W., Winkelmann, R., Zhao, C., Zhang, T., & Zwinger, T. \(2023\). Insights into the vulnerability of Antarctic glaciers from the ISMIP6 ice sheet model ensemble and associated uncertainty. \*The Cryosphere\*, 17\(12\), 5197-5217. <https://doi.org/10.5194/tc-17-5197-2023>](#)

820

- 825 Tokarska, K. B., Stolpe, M. B., Sippel, S., Fischer, E. M., Smith, C. J., Lehner, F., & Knutti, R. (2020). Past warming trend constrains future warming in CMIP6 models. *Science Advances*, 6(12), eaaz9549. <https://doi.org/10.1126/sciadv.aaz9549>
- van der Linden, E. C., Le Bars, D., Lambert, E., & Drijfhout, S. (2023). Antarctic contribution to future sea level from ice shelf basal melt as constrained by ice discharge observations. *The Cryosphere*, 17(1), 79-103. <https://doi.org/10.5194/tc-17-79-2023>
- 830 Van Der Veen, C. J., Stearns, L. A., Johnson, J., & Csatho, B. (2014). Flow dynamics of Byrd Glacier, East Antarctica. *Journal of Glaciology*, 60(224), 1053-1064. <https://doi.org/10.3189/2014JoG14J052>
- van Pelt, W. J. J., & Oerlemans, J. (2012). Numerical simulations of cyclic behaviour in the Parallel Ice Sheet Model (PISM). *Journal of Glaciology*, 58(208), 347-360. <https://doi.org/10.3189/2012JoG11J217>
- 835 van Wessem, J. M., van de Berg, W. J., Noël, B. P. Y., van Meijgaard, E., Amory, C., Birnbaum, G., Jakobs, C. L., Krüger, K., Lenaerts, J. T. M., Lhermitte, S., Ligtenberg, S. R. M., Medley, B., Reijmer, C. H., van Tricht, K., Trusel, L. D., van Ulf, L. H., Wouters, B., Wuite, J., & van den Broeke, M. R. (2018). Modeling the climate and surface mass balance of polar ice sheets using RACMO2 – Part 2: Antarctica (1979–2016). *The Cryosphere*, 12(4), 1479-1498. <https://doi.org/10.5194/tc-12-1479-2018>
- 840 Winkelmann, R., Martin, M. A., Haseloff, M., Albrecht, T., Bueler, E., Khroulev, C., & Levermann, A. (2011). The Potsdam Parallel Ice Sheet Model (PISM-PIK) – Part 1: Model description. *The Cryosphere*, 5(3), 715-726. <https://doi.org/10.5194/tc-5-715-2011>
- Wright, A. P., Young, D. A., Roberts, J. L., Schroeder, D. M., Bamber, J. L., Dowdeswell, J. A., Young, N. W., Le Brocq, A. M., Warner, R. C., Payne, A. J., Blankenship, D. D., van Ommen, T. D., & Siegert, M. J. (2012). Evidence of a hydrological connection between the ice divide and ice sheet margin in the Aurora Subglacial Basin, East Antarctica. *Journal of Geophysical Research: Earth Surface*, 117(F1). <https://doi.org/10.1029/2011jf002066>
- 845 Wyser, K., Kjellström, E., Koenigk, T., Martins, H., & Döscher, R. (2020). Warmer climate projections in EC-Earth3-Veg: the role of changes in the greenhouse gas concentrations from CMIP5 to CMIP6. *Environmental Research Letters*, 15(5), 054020. <https://doi.org/10.1088/1748-9326/ab81c2>
- 850 Zhao, C., Gladstone, R., Zwinger, T., Gillet-Chaulet, F., Wang, Y., Caillet, J., Mathiot, P., Saraste, L., Jager, E., Galton-Fenzi, B. K., Christoffersen, P., & King, M. A. (2025). Subglacial water amplifies Antarctic contributions to sea-level rise. *Nature Communications*, 16(1). <https://doi.org/10.1038/s41467-025-58375-4>
- Zhang, T., Colgan, W., Wansing, A., Løkkegaard, A., Leguy, G., Lipscomb, W. H., & Xiao, C. (2024). Evaluating different geothermal heat-flow maps as basal boundary conditions during spin-up of the Greenland ice sheet. *The Cryosphere*, 18(1), 387-402. <https://doi.org/10.5194/tc-18-387-2024>
- 855 Zwally, H., Jay, M. B. G., Matthew A. Beckley, & Jack L. Saba. (2012). Antarctic and Greenland Drainage Systems. *GSFC Cryospheric Sciences Laboratory*.